



High power pulsed magnetron sputtering: A review on scientific and engineering state of the art

K. Sarakinos ^{a,*}, J. Alami ^{b,1}, S. Konstantinidis ^{c,1}

^a Materials Chemistry, RWTH Aachen University, 52074 Aachen, Germany

^b Sulzer Metaplas GmbH, Am Böttcherberg 30-38, 51427, Bergisch Gladbach, Germany

^c Laboratoire de Chimie Inorganique et Analytique, Université de Mons, Avenue Copernic 1, 7000 Mons, Belgium

ARTICLE INFO

Article history:

Received 31 March 2009

Accepted in revised form 6 November 2009

Available online 19 January 2010

Keywords:

HPPMS

HiPIMS

Ionized PVD

ABSTRACT

High power pulsed magnetron sputtering (HPPMS) is an emerging technology that has gained substantial interest among academics and industrials alike. HPPMS, also known as HiPIMS (high power impulse magnetron sputtering), is a physical vapor deposition technique in which the power is applied to the target in pulses of low duty cycle (<10%) and frequency (<10 kHz) leading to pulse target power densities of several kW cm⁻². This mode of operation results in generation of ultra-dense plasmas with unique properties, such as a high degree of ionization of the sputtered atoms and an off-normal transport of ionized species, with respect to the target. These features make possible the deposition of dense and smooth coatings on complex-shaped substrates, and provide new and added parameters to control the deposition process, tailor the properties and optimize the performance of elemental and compound films.

© 2009 Elsevier B.V. All rights reserved.

Contents

| | |
|---|------|
| 1. Introduction | 1662 |
| 2. HPPMS: power supplies and processes | 1662 |
| 3. Plasma dynamics in HPPMS | 1664 |
| 3.1. On the HPPMS plasma | 1664 |
| 3.2. Determination of plasma properties: a theoretical overview | 1665 |
| 3.3. The HPPMS plasma properties | 1666 |
| 3.3.1. The effect of the pulse on/off time configuration on the plasma properties | 1668 |
| 3.3.2. Rarefaction in the HPPMS plasma | 1669 |
| 3.4. Instabilities in the HPPMS plasma | 1671 |
| 3.4.1. Plasma instabilities: an overview | 1671 |
| 3.4.2. Plasma initiation and the relationship between plasma instabilities and the charge transport in the HPPMS plasma | 1671 |
| 4. Plasma-surface interactions and deposition rate | 1673 |
| 4.1. Non-reactive HPPMS | 1673 |
| 4.1.1. Target-plasma interactions and target erosion rate | 1673 |
| 4.1.2. Transport of ionized sputtered species | 1675 |
| 4.2. Reactive HPPMS | 1675 |
| 5. Growth of thin films by HPPMS | 1676 |
| 5.1. HPPMS use for deposition on complex-shaped substrates | 1676 |
| 5.2. Interface engineering by HPPMS | 1677 |
| 5.3. The effect of HPPMS on the film microstructure | 1678 |
| 5.4. Phase composition tailoring of films deposited using HPPMS | 1679 |
| 6. Towards the industrialization of HPPMS | 1681 |
| 6.1. Examples of industrially relevant coatings by HPPMS | 1681 |

* Corresponding author. Tel.: +49 241 8025974, +49 2204 299390, +32 65 55 49 56.

E-mail address: sarakinos@mch.rwth-aachen.de (K. Sarakinos).

¹ All authors have contributed equally to the preparation of the manuscript.

| | |
|---|------|
| 6.2. Up-scaling of the HPPMS process | 1682 |
| 6.3. Positioning HPPMS in the coating and components market | 1682 |
| Acknowledgements | 1682 |
| References | 1682 |

1. Introduction

Thin films are used in diverse technological applications, such as surface protection and decoration, data storage, and optical and microelectronic devices. The increasing demand for new functional films has been a strong incentive for research towards not only understanding the fundamentals and technical aspects of thin film growth, but also developing new deposition techniques which allow for a better control of the deposition process. Among the various methods employed for film growth, Physical Vapor Deposition (PVD) techniques, such as magnetron sputtering, are widely used [1]. Magnetron sputtering is a plasma-based technique, in which inert gas (commonly Ar) atoms are ionized and accelerated as a result of the potential difference between the negatively biased target (cathode) and anode. The interactions of the ions with the target surface cause ejection (sputtering) of atoms which condense on a substrate and form a film [1,2]. The condensation and film growth processes frequently occur far from the thermodynamic equilibrium, due to kinetic restrictions [2,3]. Thus, a good control of both the thermodynamic and the kinetic conditions has implications on the growth dynamics and enables the tailoring of the structural, optical, electrical, and mechanical properties of the films [4]. One way to control the growth dynamics is by heating the substrate during the deposition [2]. The magnitude of the deposition temperature affects the energy transferred to the film forming species (adatoms) [2]. This energy is, for instance, decisive for the activation of surface and bulk diffusion processes [5,6] and enables control over the film morphology [7–10]. Another source of energy are the plasma particles that impinge onto the growing film transferring energy and momentum to the adatoms [4,5]. The bombarding flux consists both of neutral and charged gas particles, as well as sputtered species. Numerous studies have shown that the energy, the flux, the angle of incidence, and the nature of the bombarding species are of importance for the properties of the deposited films [4,5,11,12]. In general, the plasma particles exhibit a relatively broad energy distribution with a mean value of several eV [13]. The particle energy, and flux are affected by the target-to-substrate distance and the working pressure [1]. When the particles are charged the control of their energy can additionally be achieved by the use of electric fields, e.g. by applying a bias voltage to the substrate [4,14], while their flux depends on a number of factors including the plasma density, the target power, and the magnetic field configuration at the target [4,14]. It is therefore evident, that a high ion fraction in a depositing flux facilitates a more efficient and accurate control of the bombardment conditions providing, thus, added means for the tuning of the film properties.

In magnetron sputtering processes the degree of ionization of the plasma particles is relatively low [13], resulting in a low total ion flux towards the growing film [13]. As a consequence, in many cases bias voltage values of several tenths or even hundreds of V are required in order to increase the average energy provided to the deposited atoms and significantly affect the film properties [5]. Moreover, the degree of ionization of sputtered species is typically less than 1% [13,15,16]. As a result, the majority of the charged bombarding particles is made of Ar⁺ ions [13]. This fact in combination with the relatively high bias voltages may cause subplantation of the Ar atoms in the film [17,18], leading to a generation of lattice defects, [18,19] high residual stresses [20–23], a deterioration of the quality of the film/substrate interface [21], and a poor film adhesion [24]. Thus, the increase of the fraction of the ionized sputtered species has been an objective of many research works during the recent decades. Some of the approaches that have been demonstrated include the use of an inductively coupled plasma

(ICP) superimposed on a magnetron plasma [25], the use of a hollow cathode magnetron [25], and the use of an external ion source [26]. Parallel to the above mentioned approaches Mozgrin et al. [27], Bugaev et al. [28] and Fetisov et al. [29] demonstrated in the mid 90s that the operation of a conventional sputtering source in a pulsed mode, with a pulse duration ranging from 1 μs to 1 s and a frequency less than 1 kHz, allowed for pulsed target currents two orders of magnitude higher than the average target current in a conventional sputtering technique, such as direct current magnetron sputtering (dcMS) [27–29]. These high pulse currents resulted, in turn, in ultra-dense plasmas with electron densities in the order of 10¹⁸ m⁻³ [27–29], which are much higher than the values of 10¹⁴–10¹⁶ m⁻³ commonly obtained for dcMS [13,30]. A few years later, Kouznetsov et al. [31] demonstrated in a publication, that received much acclaim, the high power pulsed operation of the sputtered target showing that in the case of Cu the high plasma densities obtained using this pulsed technique resulted in a total ion flux two orders of magnitude higher than that of a dcMS plasma, and a sputtered material ionization of ~70%. The new deposition technique was called High Power Pulsed Magnetron Sputtering (HPPMS). In the years after Kouzsetov's report, HPPMS received extensive interest from researchers and led to a substantial increase of the HPPMS-related publications (Fig. 1). Later, several research groups [25] adopted the alternative name High Power Impulse Magnetron Sputtering (HiPIMS) for this technique.

The aim of this review paper is to describe the scientific and engineering state of the art of HPPMS. For this purpose, the principle and the basic structure of the existing HPPMS power supplies are described and the various existing approaches to produce high power pulses are demonstrated. The spatial and the temporal evolution of the HPPMS plasma and its interactions with the target and the growing film are discussed both from a theoretical and an experimental perspective. Furthermore, the effect of the HPPMS operation on the deposition rate and the film properties is presented. Finally, the use of HPPMS in industry and the challenges that the latter faces regarding the use of HPPMS are briefly addressed.

2. HPPMS: power supplies and processes

The experimental realization of HPPMS requires power supplies different than those used in conventional magnetron sputtering processes. Those power supplies must be able to provide the target with pulses of high power density (typically in the range of a few kW cm⁻²), while maintaining the time-averaged target power density in values similar to

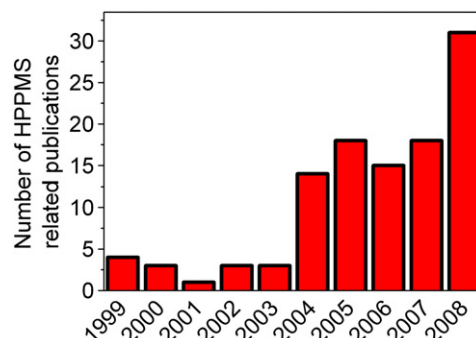


Fig. 1. Number of HPPMS-related publications in the period 1999–2008.

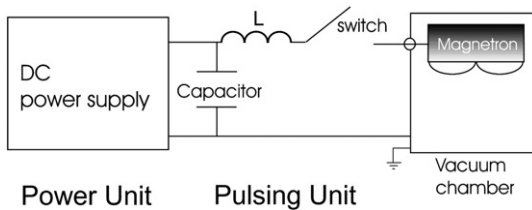


Fig. 2. Basic architecture of an HPPMS power supply. The dc generator charges the capacitor bank of a pulsing unit. The energy stored in the capacitors is dissipated into the plasma in pulses of well-defined width and frequency using ultra fast switches.

those during dcMS (i.e. a few W cm^{-2}). The low average target power density is necessary to prevent overheating of the cathode and damage of the magnets and the target. A number of research groups and companies have developed HPPMS arrangements for both laboratorial and industrial use. These devices exhibit similarities in their basic structure which is schematically depicted in Fig. 2. A dc generator is used to load the capacitor bank of a pulsing unit, which is connected to the magnetron. The charging voltage of the capacitor bank ranges typically from several hundreds of V up to several kV. The stored energy is released in pulses of defined width and frequency using transistors with a switching capability in the μs range, located between the capacitors and the cathode. The pulse width (also referred to as pulse on-time) ranges, typically, from 5 to 5000 μs , while the pulse repetition frequency spans from 10 Hz to 10 kHz. Under these conditions, the peak target current density may reach values of up to several A cm^{-2} , which are up to 3 orders of magnitude higher than the current densities in dcMS [25]. The high target current densities during the pulse on-time are accompanied by differences in the electrical characteristics of the discharge, as manifested by the current-voltage ($I-V$) curves of a magnetron operating in a dcMS and an HPPMS mode (Fig. 3). According to Thornton [32] the target and the voltage of the magnetron are linked by the power law

$$I \propto V^n \quad (1)$$

In dcMS processes the exponent n in Eq. (1) ranges from 5 up to 15 (Fig. 3). In HPPMS the exponent n changes from values similar to dcMS at low target voltages to values close to the unity when high voltages are applied (Fig. 3) [33,34].

Despite their common basic architecture, the available HPPMS power supplies exhibit differences primarily in the width and the shape of the pulses they can deliver, and in whether they can sustain a constant voltage during the pulse on-time. Arrangements able to provide high power pulses were already developed in the mid 90s, in order to explore the feasibility of producing high-current quasi-stationary magnetron glow discharges for high rate deposition [27–29]. However, it was in 1999 when Kouznetsov et al. [31] emphasized

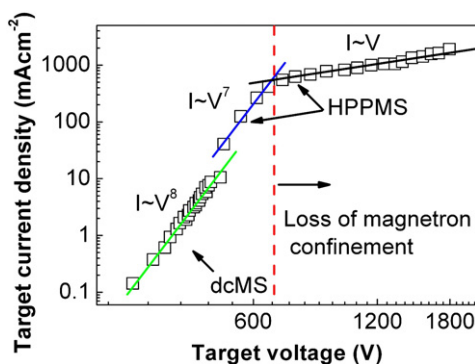


Fig. 3. Current-voltage curves of a magnetron during operation in dcMS and HPPMS mode. The change of the slope from 7 to 1 at a voltage value of 650 V indicates loss of the electron confinement (data taken from [33]).

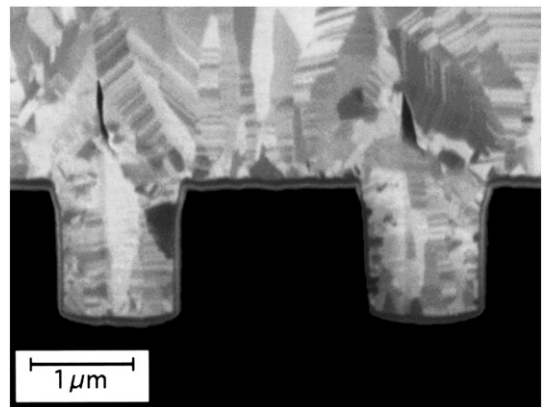


Fig. 4. Cross-section SEM image of two via holes with an aspect ratio 1:2 homogeneously filled by Cu using HPPMS (reprinted from [31] after permission, 1999 © Elsevier).

that the high power pulsing could allow for a high ionization degree of copper vapor (70%) as well as a homogeneous filling of 1:2 aspect ratio trenches (see Fig. 4). The time-dependent target current and target voltage curves of the HPPMS power supply developed by Kouznetsov et al. [31] are plotted in Fig. 5 where it is shown that the ignition of the plasma is accompanied by a drop of the voltage from ~1000 V to ~800 V, as the current increases to its peak value ranging from 200 to 230 A at the highest applied working pressure [35,36]. A characteristic of this power supply is that the loading voltage is not maintained constant during the pulse on-time, and its temporal evolution is rather determined by the size of the capacitor bank and the time-dependent plasma impedance. Other power generators were designed to deliver voltage pulses with a rectangular shape (see Fig. 6), i.e. a constant voltage value during the pulse on-time [34,37–39]. It is to be noted that pulses with widths larger than about 50 μs allow for a saturation of the discharge current and establishment of a steady-state plasma [40] provided that enough energy is stored in the capacitor bank.

A common problem encountered in sputtering processes is the occurrence of arcs. This phenomenon is particularly pronounced during the deposition from conducting targets covered by insulating layers and can be detrimental for the quality of the films, due to the ejection of μm sized droplets from the target [41,42]. The high peak target currents during the HPPMS operation may enhance the frequency of the arc events [43]. Therefore, sophisticated electronics can be used in conjunction with the HPPMS power supplies to limit their effect if formed [43]. An alternative way to alleviate this problem is to operate HPPMS using short pulses with widths ranging from 5 to 20 μs [44]. A waveform during this mode of operation is presented in Fig. 7. Within this short period of time, the glow discharge remains in a transient regime [40] (as manifested by the triangular form of the target current) so that an eventual glow-to-arc transition is prevented. These short pulses have been, for instance, shown to allow for a stable and an arc-free reactive deposition of metal oxide films [45,46]. However, in order to eliminate the time lag for plasma ignition which would allow for the production of high-current pulses within this short period of time, a pre-ionization stage has to be implemented [44,47]. The pre-ionization of the discharge ensures that a low density plasma is maintained between the pulses as the charge carriers are already present before the voltage is turned on. The plasma pre-ionization step may be achieved by superimposing a secondary plasma (such as a dc, a microwave, or an inductively coupled plasma) on the HPPMS plasma or by running the discharge at relatively high frequencies [44,47–49]. The latter pre-ionization method is extensively implemented in mid-frequency pulsed plasmas [50–53]. In contrast to the short pulses described above, long pulses with a width of several thousands of μs can also be used [54] (Fig. 8). In this case the pulse is composed of two (or more) stages. The

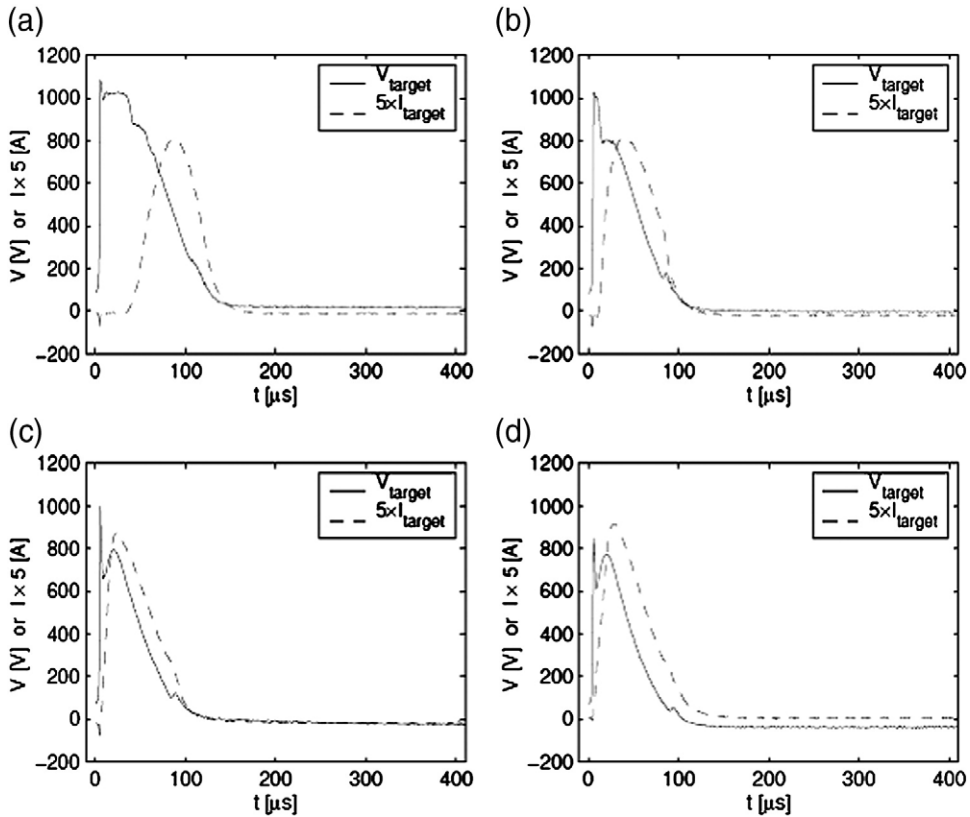


Fig. 5. Target current and voltage waveforms produced by the power supply developed by Kouznetsov et al. at working pressures of (a) 0.06 Pa, (b) 0.26 Pa, (c) 1.33 Pa and (d) 2.66 Pa. The charging voltage of 1000 V drops down to 800 V and the plasma is ignited. Peak target currents of up to 230 A are achieved. The time lag for the ignition of the plasma decreases when the pressure is increased (reprinted from [35] after permission, 2002 © Elsevier).

first step of the discharge is made of a weakly ionized regime, while the second part of the pulse brings the glow discharge to the high ionization state. The weakly ionized regime allows for the formation of a stable discharge prior to entering the highly ionized regime which helps to suppress the arc formation during the high power mode of operation [54].

3. Plasma dynamics in HPPMS

3.1. On the HPPMS plasma

Plasmas are partially ionized gases characterized by, for example, the charge (electron) density or the electron energy distribution function [55]. A classification of different plasmas could be based on the charge

density as shown in Fig. 9, where the magnetron sputtering plasmas are shown to exhibit densities ranging from $\sim 10^{14}$ up to 10^{20} m^{-3} . It is known that high density plasmas such as arc plasmas exhibit high ionization fractions [25,31]. This is not the case for conventional magnetron plasmas where the electron density does not exceed the value of 10^{16} m^{-3} , penning ionization is the main ionization mechanism [30] and therefore the ionization of the sputtered species is at the best of few percent [13]. In order to achieve a high ion fraction in a discharge it is necessary to promote the electron impact ionization [55] which is best realized by increasing the electron density and temperature. Different approaches have been made to achieve this, for example by using an electron cyclotron resonance (ECR) plasma as a plasma electron source [56], or by employing an inductively coupled plasma (ICP) [57,58]. A higher frequency of electron impact ionization collisions can also be

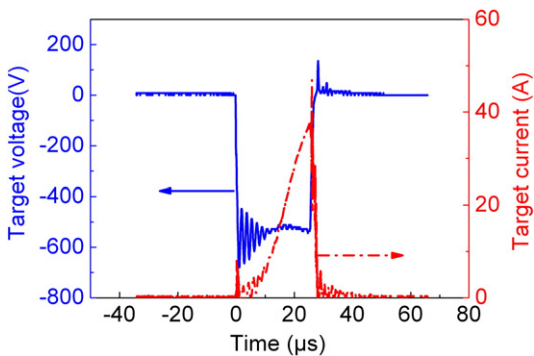


Fig. 6. Rectangular shape voltage waveforms generated by the HPPMS power supply developed by MELEC GmbH. The data were recorded from an Ar-Al HPPMS discharge operating at pulse on/off time configuration 25/475 μ s (K. Sarakinos, unpublished data).

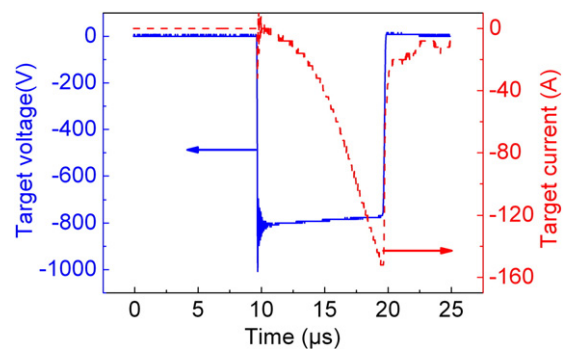


Fig. 7. Temporal evolution of target voltage and current during operation using a 10 μ s long pulse. The target current is interrupted before the plasma enters into the steady-state regime. The data were recorded from an Ar-Ti HPPMS discharge (S. Konstantinidis unpublished data).

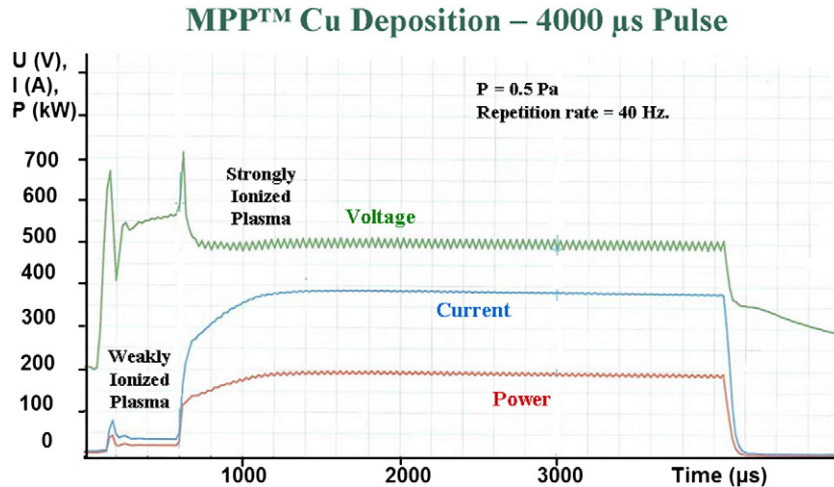


Fig. 8. Target voltage and current waveforms during the long-pulse operation. In the first 500 μ s a weakly ionized plasma is generated which is followed by a highly ionized steady-state plasma (reprinted from [54] after permission, Society of Vacuum Coaters © 2007).

achieved by increasing the power to the sputter source and therewith the electron density. This approach is, however, limited since a power excess can result in an overheating of the target or an exceeding of the Curie temperature of the magnetron's magnets. Thus, the work of Kouznetsov et al. [31] opened a new era of magnetron sputtering deposition and plasma studies, since it allowed for the generation of highly ionized plasmas using a conventional magnetron source. The early analyses of the HPPMS plasma showed that its temporal characteristics are complex and unique [35,59,60]. Understanding the discharge evolution and the mechanisms that take place in the plasma is therefore of utmost importance as this sheds light on the growth conditions during the thin film deposition. To achieve this, modeling and a number of analytical studies have been carried out, using Langmuir probes as well as optical emission, mass, and absorption spectroscopy techniques. These studies are reviewed in the following chapters and the basic properties of the HPPMS plasma are thus outlined.

3.2. Determination of plasma properties: a theoretical overview

Plasmas are commonly modeled as fluids, and each species is described with its fluid equation [61]. The fluid approximation is sufficiently accurate to describe the majority of observed plasma phenomena. When this is not viable, the accumulated behavior of an

ensemble of charged particles is described using a statistical approach, in the form of the velocity distribution function which is given as $f(\mathbf{r}, \mathbf{u}, t)d^3r d^3u$, i.e. the number of particles inside a six-dimensional phase space volume $d^3r d^3u$ at (\mathbf{r}, \mathbf{u}) and time t [55]. Here, \mathbf{r} is the position vector and \mathbf{u} is the speed vector. Knowing the distribution function, fundamental features of a large ensemble can be quantified, i.e. by integrating over the velocity, the average (macroscopic) quantities associated with the plasma are defined as:

$$n(\mathbf{r}, t) = \int f(\mathbf{r}, \mathbf{u}, t) d\mathbf{u} \text{ plasma number (ion, electron, or neutral) density} \quad (2)$$

$$\bar{\mathbf{u}}(\mathbf{r}, t) = \frac{1}{n} \int \mathbf{u} f(\mathbf{r}, \mathbf{u}, t) d\mathbf{u} \text{ plasma bulk fluid velocity} \quad (3)$$

$$\bar{e}(\mathbf{r}, t) = \frac{m}{2n} \int (\bar{\mathbf{u}} - \mathbf{u})^2 f(\mathbf{r}, \mathbf{u}, t) d\mathbf{u} \text{ plasma mean kinetic energy} \quad (4)$$

where m is the particle (ion, electron, or neutral) mass. This procedure of integrating over velocity space is referred to as taking velocity moments, with each one yielding a physically significant quantity. Knowledge of the electron energy (velocity) distribution function (EEDF) permits us to determine important parameters. The EEDF can be measured using a Langmuir probe, as was demonstrated by Druyvesteyn [55]:

$$g_e(V) = \frac{2m}{e^2 A_{pr}} \left(\frac{2eV}{m} \right)^{\frac{1}{2}} \frac{d^2 I_e}{dV^2} \quad (5)$$

where A_{pr} is the probe area, I_e is the electron current, m is the electron mass, and $V = V_{pl} - V_b$ is the potential difference between the plasma potential and the probe potential. With the change of variables $\varepsilon = eV$, the electron density n_e is determined as:

$$n_e = \int_0^\infty g_e(\varepsilon) d\varepsilon \quad (6)$$

Plasma parameters, such as the electron density, are easily obtained if the mathematical description of the EEDF is Maxwellian. The Maxwellian distribution is characterized by its single temperature and is obtained when plasma electrons undergo enough collisions and are in equilibrium with other plasma components and with the electron ensemble itself. At a low pressure, the EEDF is generally non-Maxwellian, and the electron temperature is thought of as an effective

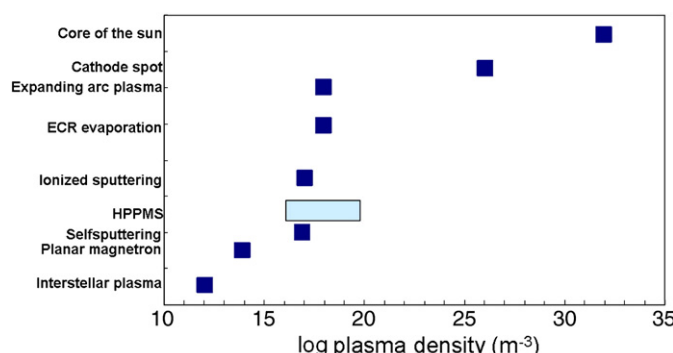


Fig. 9. Plasma density is used in order to classify plasmas. The HPPMS plasma spans over a large density range depending on the pulse on/off time configuration used for a process and presents therefore a tool for better choosing the plasma dynamics needed for the deposition process. The abbreviation ECR stands for Electron Cyclotron Resonance (taken from [36]).

electron temperature, $T_{\text{eff}} \sim \frac{2}{3}\langle \varepsilon \rangle$, representing the mean electron energy determined from the EEDF according to [55]:

$$\langle \varepsilon \rangle = \frac{1}{n_e} \int_0^\infty \varepsilon g_e(\varepsilon) d\varepsilon \quad (7)$$

3.3. The HPPMS plasma properties

One of the earliest works related to the study of the properties of the HPPMS plasma was carried out by Gudmundsson et al. [35,59]. Using a Langmuir probe [62] in an Ar-Ta plasma, they measured the temporal behavior of the EEDF by recording the time-dependent probe current curves. It was shown that the EEDF evolved from a Druyvesteyn-like distribution with a broad energy distribution (high

average energy) during the pulse to a double Maxwellian distribution (i.e. a distribution that is composed of two-distinct energy-distributions) toward the end of the pulse, and finally a Maxwellian-like distribution hundreds of μs after the pulse had been switched off. This is shown in Fig. 10, where the temporal evolution of the EEDF is also seen to be affected by the working pressure [35]. Similar results were obtained by Pajdarova et al. [63], although the double Maxwellian distribution was observed from the beginning of the pulse, which could be explained by the nature of the target material (Cu in this case) and the HPPMS parameters used in the experiments. Furthermore, it was found that the effective electron temperature peaked a few μs after the pulse start, and at the same time, independent of measurement position [35]. This is indicative of the existence of high energy electrons accelerated by the target voltage, and thus escaping the confinement region in the vicinity of the cathode [35]. In a

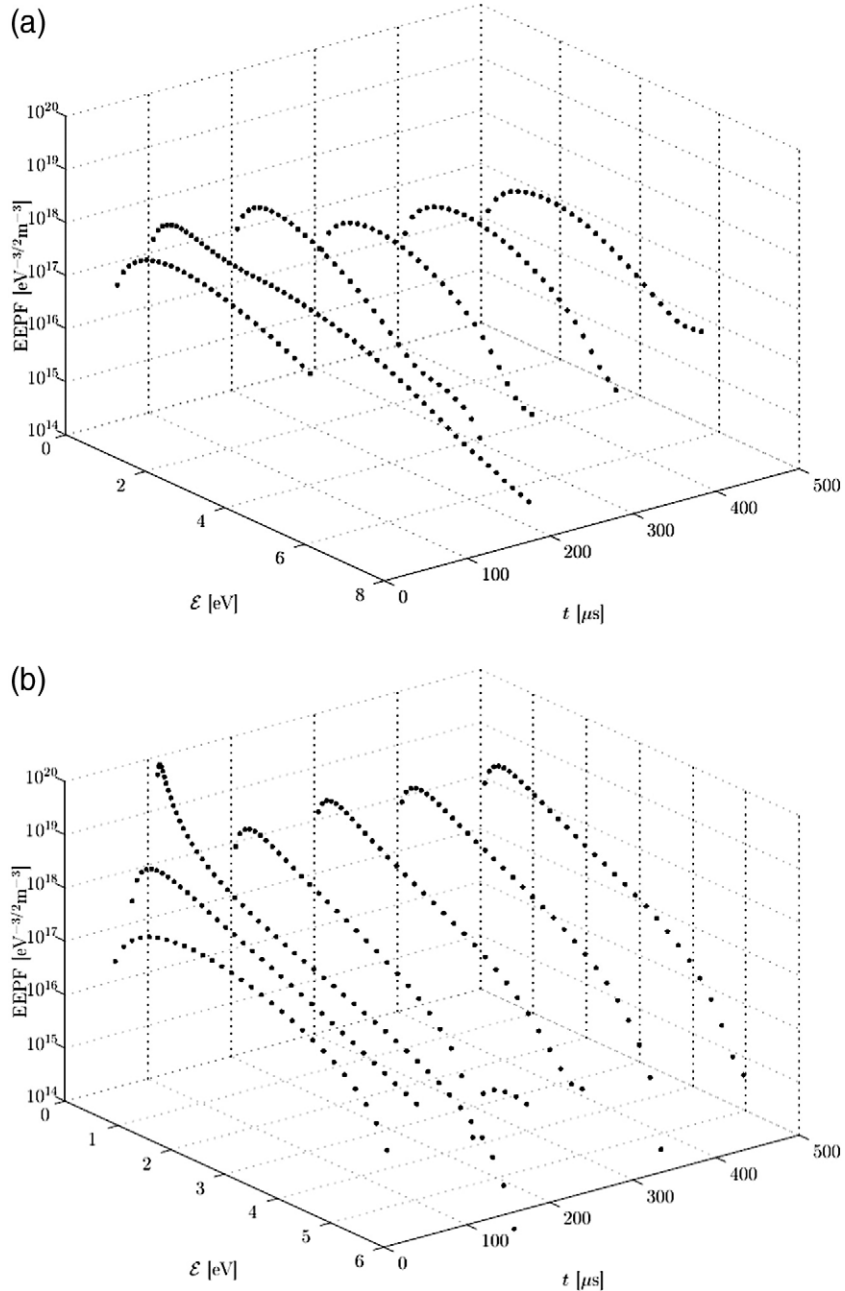


Fig. 10. The EEDF (electron energy distribution function) for an HPPMS plasma with a 100 μs on-time and a 50 Hz frequency at three chamber pressures (a) 0.25, (b) 1.33, and (c) 2.66 Pa. The distribution function changes during the pulse from a Druvesteyn distribution to a double-Maxwellian distribution (reprinted from [35] after permission, Elsevier © 2002).

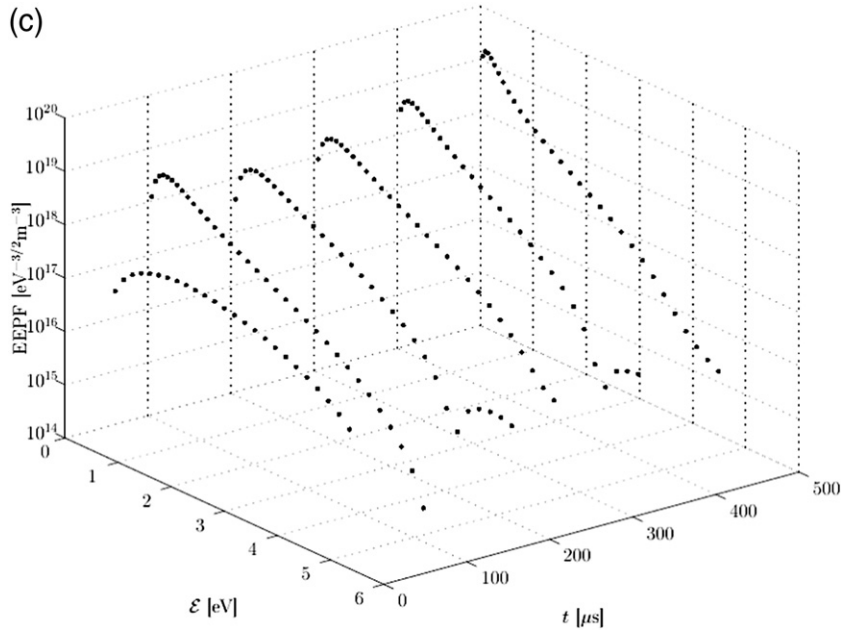


Fig. 10 (continued).

different study by Seo et al. [64], Langmuir probes were utilized to determine the properties of a HPPMS plasma at a higher pulsing frequency of 10 kHz and a duty cycle of 10%. By using such a high frequency, the electron density reached a value of $1.5 \times 10^{17} \text{ m}^{-3}$, which could be seen as a relatively low density HPPMS plasma. The temporal evolution of the energy distribution in this plasma showed efficient electron heating, which took place within the first few μs from the pulse start. This work revealed that the plasma dynamics presented in the studies by Gudmundsson et al. [35,59] are to a large extent general features of the low duty cycle pulsed plasmas regardless of the frequency.

The early studies on the HPPMS plasma characteristics also showed the potentially high ionization fraction of the sputtered material that could be achieved by using this technique [16,25,33,60,65,66].

Spectroscopic analyses, such as optical emission spectroscopy [67–69], mass spectroscopy [69], and absorption spectroscopy [68,69] were, therefore, employed in order to better quantify and understand the average and time-dependent evolution of the ion population in the HPPMS plasma. The optical emission studies [33,65,70–72], were performed both for the HPPMS and the dcMS discharges and showed the much higher metal ion emission intensity in HPPMS (Fig. 11). However, in order to better quantify these observations, absorption spectroscopy [70,71,73,74] and mass spectroscopy [75,76] studies were performed, confirming the much higher ionization of the sputtered material and of the sputtering gas achieved in HPPMS. One well studied material in this regard is Ti. Mass spectroscopy measurements of the peak ion compositions in an Ar-Ti discharge for the pulse on-time of 100 μs and a frequency of 50 Hz [75] showed that the ionized part of the plasma contained 50% of Ti^{1+} , 24% of Ti^{2+} , 23% of Ar^{1+} , and 3% of Ar^{2+} ions. When longer pulse on-times of several hundreds of μs were used even Ti^{3+} and Ti^{4+} could also be detected [77]. It is deduced that for the formation of multiply charged ions certain conditions should be fulfilled [77]; (i) the discharge should contain a high enough number of metal ions, (ii) the pulse on-time should be long enough (and the capacitance of the used power supply should be large enough to store enough energy for the whole pulse), (iii) the self-sputtering yield (i.e. the sputtering yield of the target material from ionized target species) should be low, and (iv) the ionization energy of each ionization step should not be too high. These two examples show clearly that the HPPMS plasma properties depend not only on the plasma density and energy distribution but also, to a large degree, on the pulse on/off time configuration.

Since the introduction of the HPPMS technique, most of the discharge studies have been performed for pulses with pulses on-time longer than 50 μs . Exceptions to this can be found in the works by Konstantinidis et al. [70,73], Ganciu et al. [44], and Vasina et al. [48], where shorter pulses ranging between 5 and 30 μs have been used, an example of which is shown in Fig. 7. Using time-resolved optical emission spectroscopy in a Ti-Ar discharge, an increase in the line intensity ratio of the ion-to-neutral Ti and Ar species with increasing the pulse duration was observed [70]. This means that the ionization degree increases with increasing pulse length, indicating the necessity for the sputtered atoms to reside a sufficient time in the target vicinity for the vapor to become ionized. The increase of the Ar emission

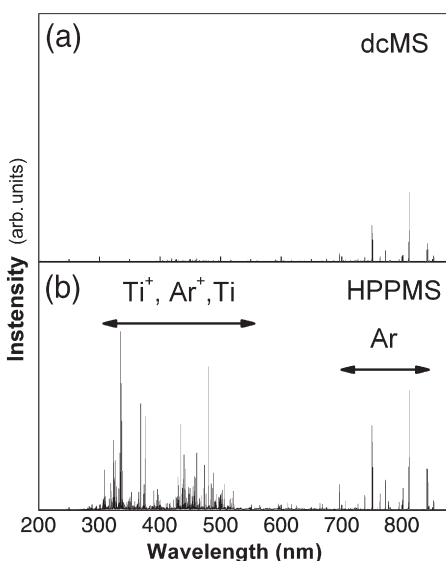


Fig. 11. Optical emission spectroscopy from a typical HPPMS plasma. The emission from the Ti and Ar species increases greatly in HPPMS indicating the high ionization of the metal and gas species (data taken from [72]).

intensity demonstrates that by using very short pulses, the density in the HPPMS discharge can be increased while refraining it from evolving into a steady-state plasma [70] and thus some of the observed phenomena in HPPMS plasmas with pulse on-time larger than 50 μ s do not occur [34,39].

3.3.1. The effect of the pulse on/off time configuration on the plasma properties

The choices of pulse on-time and frequency were not available options in the power supply when the HPPMS technology was first introduced. This means that, when using HPPMS, the only reference was with respect to the single on/off time configuration provided by the power supply developed by Kouznetsov et al. [31], i.e. 50–100 μ s on-time and 20 ms off-time. Soon, new power supplies were introduced with added features, as described in Section 2. More attention began to be paid to the length of the pulse on- and off-times as these were among the main contributing factors to the observed plasma dynamics. The change of the pulse on/off time configuration entails major changes to the target voltage and average current. Furthermore, by keeping one of these values constant, for example the average target current, it is possible to see the effect of the pulse configuration change on the peak target current and voltage. This is illustrated in Fig. 12 where it is shown that, by increasing the pulse off-time, both the target voltage and the peak target current increase. Besides, the shape of the target current is no longer the same. These changes can only be explained in the context of the temporal evolution of the HPPMS plasma [34,35,59,70] which is discussed in the following sections. It is clear, however, that a change of the pulse on/off time configuration would influence both the target voltage and the peak target current, even if the power is kept constant, which means that a comparison to a dcMS discharge of an equal power is only valid for the chosen configuration. Konstantinidis et al. [70] investigated this issue for short pulses with an on-time smaller than 50 μ s using a constant average power. By keeping the average power and increasing the pulse on-time from 5 to 20 μ s, the discharge was shown to evolve from an Ar-sputtering to self-sputtering discharge. This had also implications on the deposition rate, as will be discussed in Section 4 of the present review. Alami et al. [34] took a different approach when investigating the effect of the pulse on/off time configuration on the discharge dynamics keeping the average target current (which has a linear effect on the sputtering rate) constant. This approach, which was taken in order to gain better insight on the plasma transformations resulting from the choice of pulse on- and off-times, showed that one of the main factors which define the

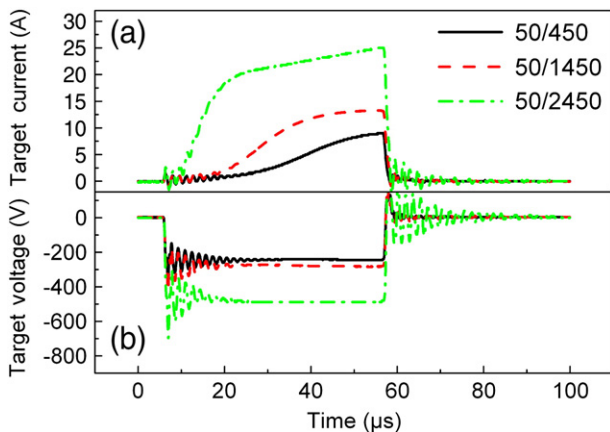


Fig. 12. The effects of the pulse on/off time configuration on the HPPMS process: an increase of the pulse off-time results in an increase of the target voltage and peak target current as well as a change of the current curve shape (K. Sarakinos, unpublished data).

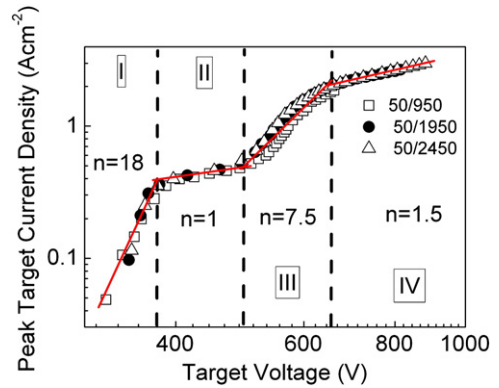


Fig. 13. The effect of the pulse on/off time configuration on the HPPMS process: the value n of the exponential relationship between the target voltage and the peak target current ($I \sim V^n$) changes as a function of the peak target current (or voltage) and is independent of the pulse on/off time configuration. The n value is high ($n = 18$) for low power and low peak target current plasmas, which is typical for a dc-like plasma (I). At a well-defined peak target current the value n becomes equal to unity indicating an increased plasma impedance (II). The value n increases further to 7.5 which is explained as the result of the increased ionization (III). Finally at peak target currents higher than 1.6 A cm^{-2} the magnetic confinement (induced by the high azimuthal current which in turn results in a high induced magnetic field that screens the effect of the magnetron's field) is lost and n is once again close to the value 1 (data taken from [34]).

properties of the HPPMS plasma is the peak target current. It was shown that for a Cr target, independent of the pulse on/off time configuration, at a well-defined peak target current density value of 0.36 A cm^{-2} , the plasma changed from a dcMS-like plasma to HPPMS-like as manifested by the relationship between the target voltage and the peak target current (Fig. 13). In other words, the relationship between the target voltage and peak current changed considerably, while an intensified depletion of the working gas species from the target vicinity, i.e. rarefaction [78], was observed (Fig. 14). The rarefaction effect, which is discussed in more detail in Section 3.3.2, resulted in an increase of the plasma impedance, in agreement with Rossnagel's description of this phenomenon [78]. At a higher peak target current density value of $\sim 0.57 \text{ A cm}^{-2}$ (again independent of the pulse on/off time configuration), the effects of self-sputtering

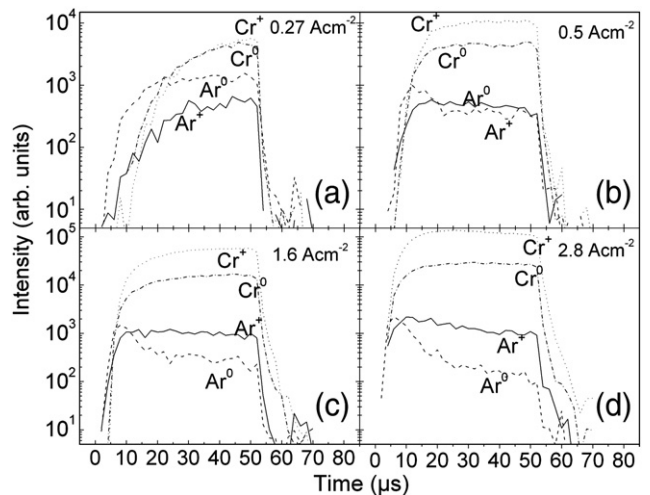


Fig. 14. The rarefaction effect as manifested by optical emission spectroscopy measurements. At the lowest peak target current (a) an increase of the ionized species emission signal is detected. The increase continues for the Cr species when the peak target current increases but not for the Ar species (b). A further increase (c) shows that the Ar signal starts to decrease manifesting the rarefaction of these species. For the highest peak current (d) the rarefaction is well established. Note that the intensity scale is not the same for all parts of the figure (data taken from [34]).

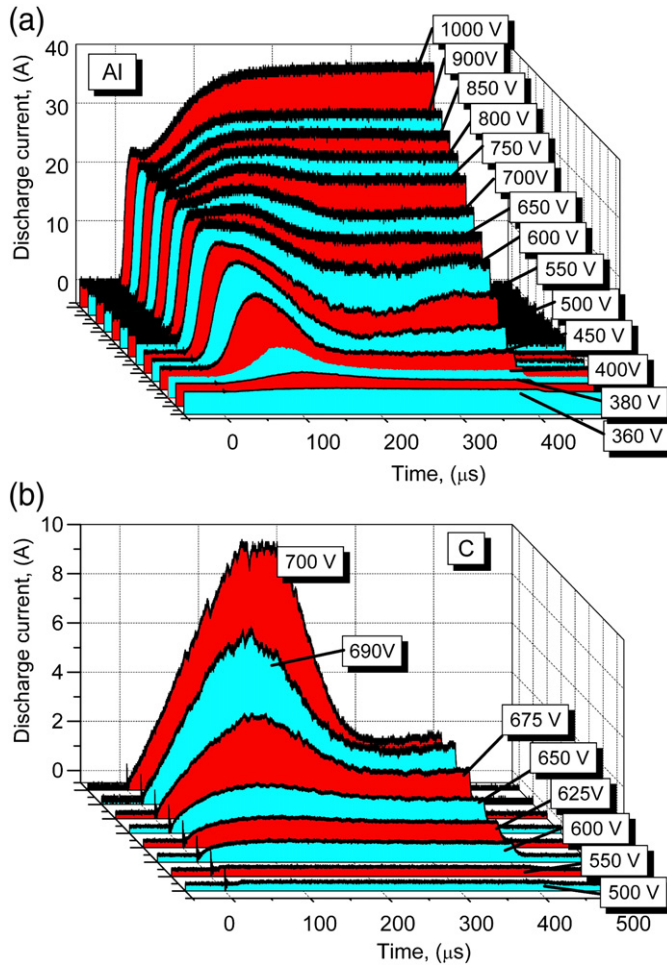


Fig. 15. Current pulse shapes at different constant target voltages for (a) Ar-Al and (b) Ar-C HPPMS discharges. In the case of the Al target and above a certain voltage limit the target current is sustained at a high level throughout the pulse indicating a self-sustained self-sputtering. This is not possible for the C target due to the low sputtering yield and the high ionization potential of this material (reprinted from [39] after permission, American Institute of Physics © 2007).

(sputtering by the target metal ions) became dominant, which was followed by a large decrease of the plasma impedance (Fig. 13). It was also only at this point that the deposition rate deviated from the rates measured for dcMS, which will be illustrated in more detail in Section 4.

The effect of different pulse lengths on the properties of the HPPMS plasma was further investigated by Anders et al. [39], where they showed that by using long pulses of up to 400 μs and a target material with high self-sputtering yield, the discharge was given the time to evolve into a metal discharge phase dominated by self-sputtering of the target, which eventually led to a strong generation of multiply charged particles [77] and, under certain conditions, to a substrate ion current larger than discharge current [79]. The transition of the discharge into a self-sputtering mode is illustrated in Fig. 15(a) for an Al-Ar plasma where it is seen that at a well-defined target voltage, the plasma changes in character and a new steady state is found. This is not the case in an Ar-C plasma (Fig. 15(b)), where the low sputtering yield and the high ionization potential of C do not allow for the discharge to evolve into the self-sputtering mode. Furthermore, Anders et al. [39] found that the current evolution during the pulse depends not only on the power and the pulse configuration used at the target but also on the secondary electron emission of the target. It is known that part of the current driven to the magnetron is carried by electrons ejected from the target during the sputtering process, i.e. the

secondary electrons. The secondary electrons affect the ion target current density j_i as [80]

$$j_i = \frac{j_{\text{Tav}}}{1 + \gamma_{\text{SE}}} \quad (8)$$

where γ_{SE} is the secondary electron emission yield and j_{Tav} is the average target current density. The value of γ_{SE} depends on the nature of the target material and the sputtering ions, as well as the energy of the sputtering ions. For ion energies below 1 keV (which is the case for most common sputtering processes) γ_{SE} is independent of the ion energy and the generation of secondary electrons takes place via a mechanism known as potential emission [81–83]. In this case γ_{SE} can be calculated by the empirical expression [81],

$$\gamma_{\text{SE}} = 0.032(0.78E_{\text{pot}} - 2\phi) \quad (9)$$

where E_{pot} is the ionization potential of the impinging ion and ϕ is the work function of the target material. For singly charged metal ions (e.g. Ti^+ , Cr^+ , Cu^+) E_{pot} is typically smaller than 2ϕ [84], which implies that these ions cannot induce potential emission of secondary electrons (see Eq. (9)). When multiply charged metal ions are involved in the sputtering process, they impinge on the cathode with energies typically higher than 1 keV. In this case γ_{SE} depends on the energy of the impinging ions and the ejection of secondary electrons is facilitated via a mechanism known as kinetic emission [82]. Moreover, multiple charged metal ions typically exhibit ionization potentials higher than 2ϕ , which means that potential emission can take place [85]. The latter in combination with kinetic emission may compensate the loss of secondary electrons induced by the presence of singly charged target species in the ion flux to the target. In any case, the effect of secondary electrons on the ion target current should also be taken into account, when the plasma-target interactions in HPPMS are treated.

3.3.2. Rarefaction in the HPPMS plasma

The concept of rarefaction has been explained in the works of Rossnagel and Hoffman [86,87]. There, they showed, using pressure probe measurements, that a reduction of the local gas density in the vicinity of the target takes place during magnetron sputtering. They explained this to be the result of gas heating by the energetic sputtered atoms through collisions and thermalization of the sputtered atoms (Hoffman named this phenomenon “sputtering wind” [87]). Furthermore, the resulting rarefaction was shown to be stronger with heavier background gas (since it has a higher sputtering yield and a lower thermal conductivity), and with higher target current (as more atoms are sputtered). The effect of the rarefaction on the dynamics of the HPPMS plasma has been studied experimentally by OES measurements [33,34,70] and modeled by Kadlec [88] using Monte Carlo simulation. The simulation results are depicted in Fig. 16, where the temporal evolution of the gas mixture in the area in front of the sputter target is shown. It was concluded that the gas rarefaction is very strong in HPPMS and manifests itself as rapid moving shock waves that start a few μs after the beginning of the pulse. Furthermore the simulation showed that the volume density of the sputtered metal exceeds the gas density several times. Despite the simplified approach that the Kadlec model takes, it agrees very well with the optical emission spectroscopy findings in the target vicinity by other researchers [33,34,70]. An example is given in Fig. 14 where Cr and Ar neutrals and ions evolutions from the pulse start until the pulse end are monitored. The rarefaction is manifested here by the decrease of the Ar ions and especially neutrals emission signal as the peak target current was increased (the pulse off time was increased) [34]. This should, however not be seen as an absolute measure of the rarefaction as the Ar emission signal would also be reduced if the electrons are

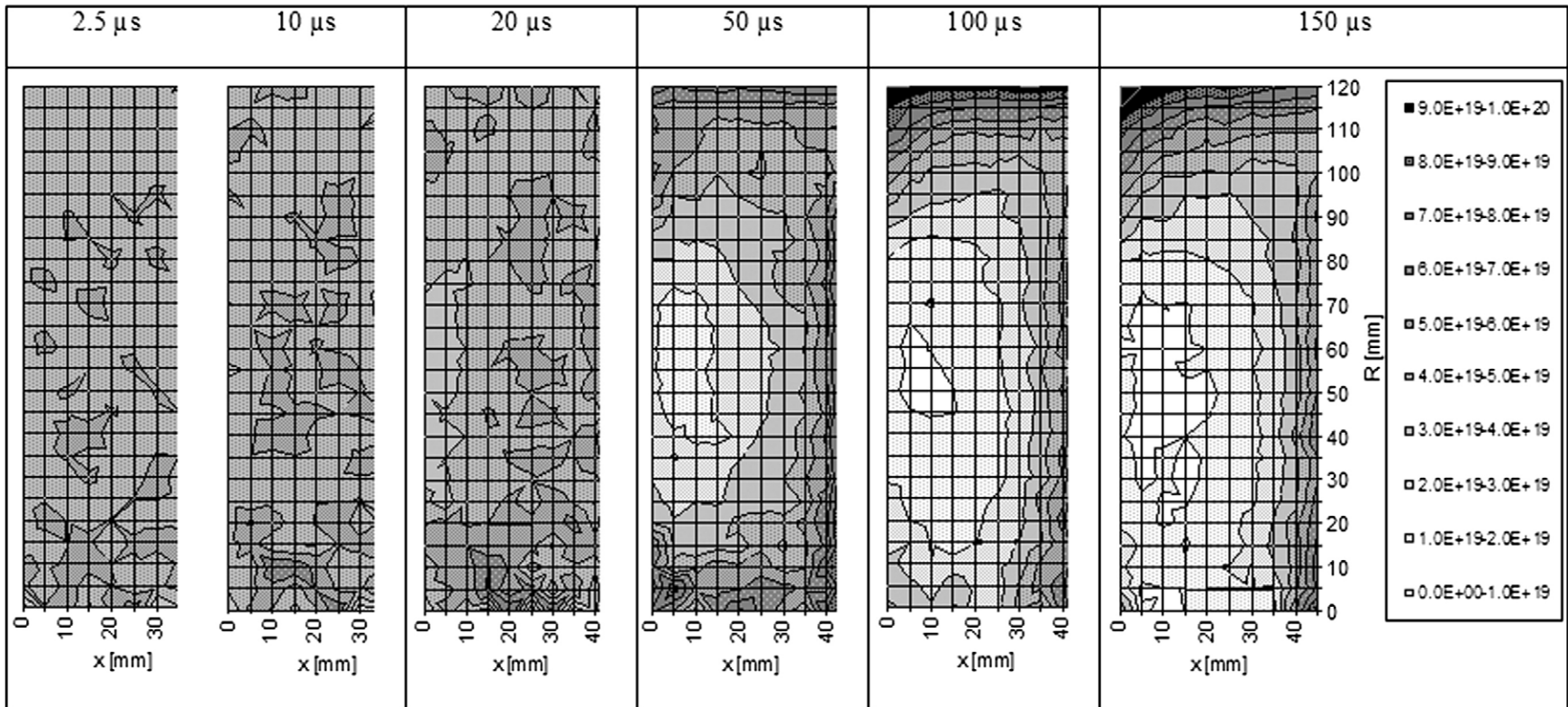


Fig. 16. The rarefaction effect modeled as the time evolution of number density of Ar gas. After 20 μ s the gas density decreases in front of the target erosion zone. The trend continues with time, leaving the main space rarefied (reprinted from [88] after permission, Wiley-Interscience © 2007).

cooled by the sputtered metal and are unable to ionize and/or excite as efficiently.

3.4. Instabilities in the HPPMS plasma

3.4.1. Plasma instabilities: an overview

Plasmas, unlike ordinary gases, support a wide variety of wave modes because of the charged particles. An example of these wave-like disturbances is the ion acoustic wave which is an electrostatic wave occurring in an *a priori* field free plasma, magnetosonic waves, and electromagnetic waves, which can typically be described by an electric field of the form $E(x, t) = E_0 \exp[i(kx - \omega t)]$, where E_0 and ω are the complex amplitude and angular frequency, respectively [61] and k is the wave vector. If the wave is electromagnetic in nature then the magnetic field obeys a similar relation as well [61]. The (angular) frequency ω and the wave vector are functionally related to one another, at least in linear theories of plasma waves, through a dispersion relationship $\omega(\mathbf{k})$. Knowledge of the dispersion characteristics of the propagating waves is certainly necessary for an understanding of the plasma state. Plasma, however, is a non-linear medium and unless the waves are truly of small amplitude, non-linear effects must be taken into account. Such non-linear effects conspire to produce wave-like disturbances that are not of the form given above [61].

One of the factors behind the non-linear behavior of the plasma waves is the two-stream instability which is a very common instability in many plasma experiments [89,90]. It can be induced by an energetic particle stream injected in the plasma, or by setting a current along the plasma so that ions and electrons can have different drift velocities. The relative drifts between electrons (u_e) and ions (u_i) in the plasma, i.e. $u_{\text{rel}} = u_i - u_e$, in the presence of a magnetic field component perpendicular to this relative drift is technically known as the modified two-stream instability (MTSI), and causes charge perturbation which can lead to plasma wave excitation. This is the case for the circulating Hall current in the magnetic field trap of a magnetron above the target in a discharge [91]. Because the ion gyro radii in magnetrons are typically larger than the spatial dimension of the plasma, only the electrons are considered to be magnetized and take part in this azimuthal drift. If the wave electric field has a small but finite component along the magnetic field, the electrons will not only Hall drift transverse to the **E** and **B** fields but also be accelerated along the magnetic field [92].

3.4.2. Plasma initiation and the relationship between plasma instabilities and the charge transport in the HPPMS plasma

3.4.2.1. Ion acoustic solitary waves in the HPPMS plasma. The plasma studies made to date have been focused on the one aspect or the other of the plasma stage. In the present section, inspired by these studies, an attempt is made at explaining the temporal evolution of the HPPMS plasma.

As already stated, the pulses in the HPPMS plasma are short and far in between. The plasma, as a result, manages to be switched on during the pulse on-time and extinct during the pulse off-time. Therefore, the understanding of the plasma dynamics only requires the study of the plasma state during one pulse. It is clear that the plasma starts from a background where no charges or electrical fields are present, which means that the plasma impedance transits from a very high value during the pulse off-time to a much lower during the pulse on-time [34]. In order to illustrate this effect, consider a large water tank placed at a certain height with respect to a reservoir. Consider further that the tank has a large door that could open instantly. When the door opens, the tank could be emptied fast which would result in a shock impact on the reservoir and a number of perturbations. Analogically, the HPPMS discharge starts by opening the gates (pulse on) of the capacitor bank that stores a large amount of energy.



Fig. 17. Experimental reproduction of the Russell Scott solitary wave in a water canal: the boat was stopped suddenly giving rise to a single water heap that continued along the canal without changing shape or velocity.
Photo courtesy of D. B. Duncan and J. C. Eilbeck, Heriot-Watt University, Edinburgh.

The results of such an action are described in the work of Gylfason et al. [93] who showed the existence of solitary-like waves that are initiated at the target some 10 μ s after the pulse start. This shock impact on the chamber gas, which was manifested by the generation of a solitary-like wave [94–97] was reported for the first time in a sputtering plasma [93]. The discovery of solitary waves dates back to Scott Russell (1834), a Scottish scientist who was observing a boat being drawn along ‘rapidly’ by a pair of horses [98]. When the boat suddenly stopped, Russell noticed that the bow wave continued forward “at great velocity, assuming the form of a large solitary elevation, a well-defined heap of water which continued its course along the channel apparently without change of form or diminution of speed” (Fig. 17). The observations of Russell appeared to contradict the non-linear shallow-water wave theory of Airy (1845) [99], which predicted that a wave with elevations of finite amplitude could not propagate without change of form, i.e. it would steepen and eventually break. Ion acoustic solitary waves can be described as constant-velocity waves where the group velocity is equal to the phase velocity. Thus ion acoustic solitary waves are stationary pulses or wave packets that propagate in non-linear dispersive media [61].

In the HPPMS plasma, the high “shock” energy, which is manifested by the large plasma impedance gradient between the pulse off-time and the pulse on-time, is one of the conditions necessary for a solitary wave to emerge. It was shown that such an ion acoustic solitary wave can exist without the presence of an initial quiescent background plasma [93]. Furthermore, it was found that the velocity of the wave decreases with increasing pressure in the plasma chamber and that it is almost independent of the pulse energy [93]. The amplitude of the waves increased with increasing energy which showed that the observed waves were not classical mathematical solutions (solitons) to the non-linear wave equations, but could be modeled by spherically expanding solitary ion acoustic waves traveling away from the target. The generation of an ion acoustic wave at the beginning of the pulse results in a number of instabilities in the magnetic and electric fields, which take place later on in the pulse and govern the plasma behavior. The results of such instabilities are described in more detail in the next section.

3.4.2.2. Charge transport in the HPPMS plasma. During the HPPMS operation, a deformation of the magnetic field occurs. This was shown,

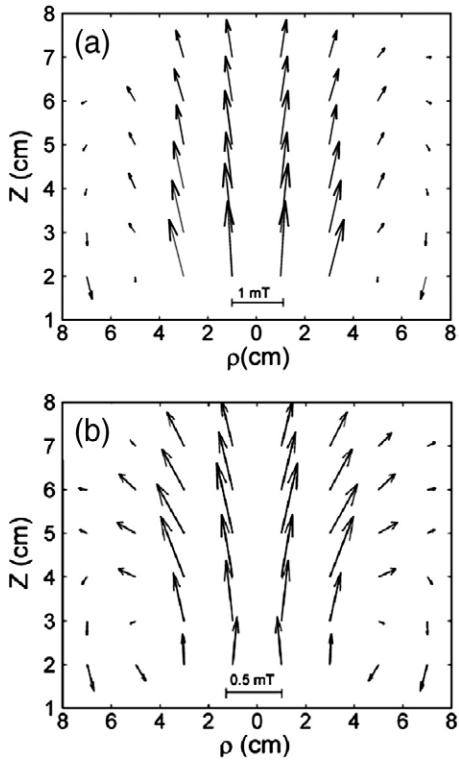


Fig. 18. The magnetic field change in the ρ - Z plane. (a) These data were taken 16 μ s after pulse ignition at 20 mTorr Ar pressure. The shape of the B -vectors indicates the presence of a circulating Hall current with its peak density around $\rho = 5$ cm, $Z = 1$ cm. For reference the length of the bar represents 1 mT. (b) The magnetic field change in the magnetron at 100 μ s after pulse ignition. The peak Hall current density has now moved to around $\rho = 5$ cm, $Z = 3$ cm. For reference the length of the bar represents 0.5 mT (reprinted from [91] after permission, Institute of Physics © 2004).

by Bohlmark et al. [91], to take place simultaneously with a large electron transport across the magnetic field lines, as shown in Fig. 18. This phenomenon cannot be explained by the classical theory of diffusion and electrical conductivity, moving electrons across the magnetic field lines using collisions, or so-called Bohm diffusion [30]. By using a coil-type magnetic probe, deformations of the magnetic field were observed in the pulsed high-current magnetron discharge. The deformations were in two stages; a first and dominant stage which occurred at an early stage of the pulse and was in phase with the axial discharge current (Fig. 18(a)), and a second stage which occurred later in the pulse, was not in phase with the discharge current (Fig. 18(b)), was described as a magnetic wave traveling from the target. In order to explain this, it was proposed [91] that the first stage of the disturbance was created by electron drifts caused by the applied electric field. This study [91] also highlighted the presence of a plasma pressure gradient close to the target and of currents driven by the curvature and gradient of the magnetic field. The second stage of the deformation took place after the applied electric field was removed, and the electron drift was attributed to the plasma pressure gradients and the curvature and gradient of the magnetic field. This type of anomalous transport was later confirmed by Lundin et al. [100,101] and Brenning et al. [102] who also discussed that it is driven by the MTSI. The development of the MTSI results in variations in the electric field, the electron, and ion densities in the MHz scale. Consequently, the resistivity of the plasma and thereby the momentum transfer between electrons and ions is perturbed, and the transport of the charged species in the plasma are affected [38,101,103,104]. This takes place in such a way that if charged particles densities are summed, then there is a net force on the charged particles resulting from the electric potential caused by the charge difference. This in turn drives the charged particles across the magnetic field lines (Fig. 19).

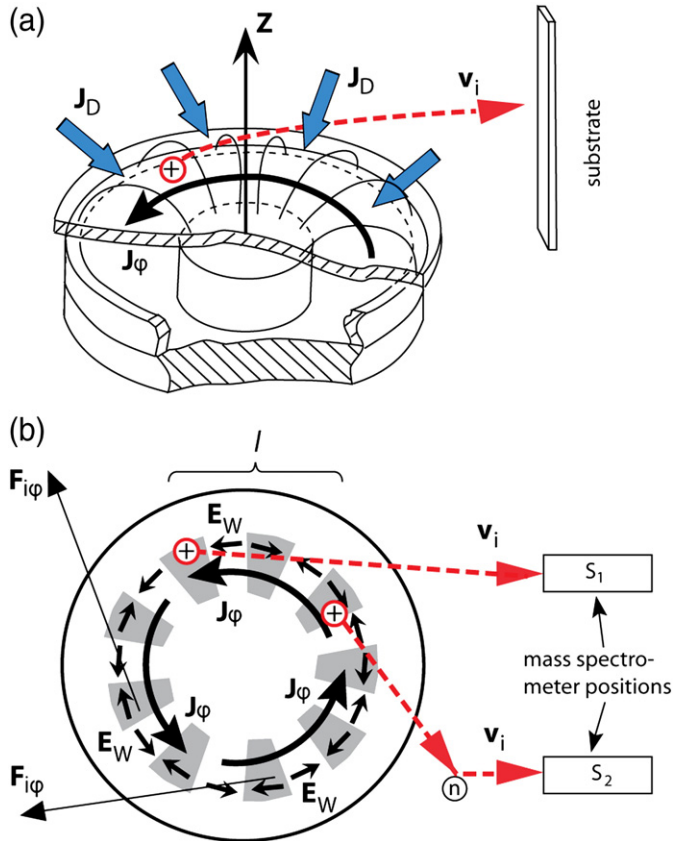


Fig. 19. The current system in a magnetron and how it is related to the sideways ion deflection. (a) The azimuthal current J_ϕ and the discharge current J_D are perpendicular to \mathbf{B} . Both exert forces on the ions. (b) Illustration of the microscopic nature of the force from J_ϕ . The dashed arrows show the deflection of ions sideways towards the substrate where the enhanced deposition rate is measured. $F_{i\phi}$ is the ion force, v_i is the ion velocity and n symbolizes the neutral background gas. E_W is the oscillating electric wave field (oscillations are indicated by grey and white stripes) found in the anomalous transport and l is the length scale which is approximately 0.05 m (reprinted from [101] after permission, Institute of Physics © 2008).

The transport dynamics of the charged particles in an HPPMS plasma could be summarized as follows:

- (i) A shock solitary ion acoustic wave is generated soon after the plasma initiation.

Table 1

HPPMS-to-dcMS deposition rate ratios for various materials.

| Material | HPPMS-to-dcMS deposition rate ratio | Reference |
|---|-------------------------------------|-----------|
| Ti | 15–75% | [25,36] |
| Cr | 29% | [25] |
| Cu | 37–80% | [25] |
| Al | 35% | [25] |
| Ta | 22–40% | [25,138] |
| Zr | 15% | [25] |
| C | 77% | [111] |
| TiSiC ^a | 60% | [158] |
| TiO ₂ ^b | 30–120% | [108,109] |
| ZrO ₂ ^b | 40% ^d | [107] |
| Ta ₂ O ₅ ^b | 106% ^d | [107] |
| Al ₂ O ₃ ^b | 25–31% | [106] |
| TiAlN ^b | 100% | [105] |

^a Deposition performed from compound target.

^b Deposition performed under the presence of reactive gas.

^c Values higher than 100% obtained during deposition from a ceramic target [107].

^d Rates compared to those obtained by pulsed magnetron sputtering at a repetition frequency of 40 kHz [106].

- (ii) This wave causes perturbations, including the MTSI, which are manifested by the plasma pressure gradient, together with the Hall drift and the magnetic curvature, which help to accelerate the ions in the azimuthal direction by interaction with the electrons, i.e. when doing the relative velocity balance between electrons and ions.
- (iii) Because of the high azimuthal current density above the race track, current density dependent volume forces are applied, which results in a tangentially outward motion of the ions.

4. Plasma-surface interactions and deposition rate

In the previous section it has been demonstrated that the HPPMS discharge provides a high density plasma with ionization degrees significantly larger than those in a conventional magnetron sputtering discharge. In the current section the interactions of the HPPMS plasmas with the target and the substrate and their effect on the deposition rate are examined. The deposition rate in HPPMS is an area that has been attracting considerable attention. It has been reported that depending on the target material, the pulse configuration and whether the deposition is performed in a non-reactive or a reactive mode, rates ranging from 15% to 120% of the values achieved by dcMS are obtained, when the same average power is used [25,70,105–111] (Table 1). Since the deposition rate is a quantity of significant technological importance, several research groups have attempted to identify mechanisms that determine its magnitude in HPPMS. In the following paragraphs, experimental and theoretical studies of the deposition rate in both non-reactive and reactive HPPMS are reviewed.

4.1. Non-reactive HPPMS

Metalization or non-reactive deposition from a metallic target is of high importance to a number of industrial applications, such as semiconductors and optical devices [112–114]. The use of HPPMS for such a process has been shown to give lower deposition rates than those obtained by dcMS at the same average target power [25,70], as demonstrated in Table 1. In order to understand the mechanisms behind this loss of deposition rate, researchers have focused their attention on two stages of the film deposition process, (i) the interactions of the plasma species with the target and their effect on the target erosion rate, and (ii) the transport of the ionized sputtered species from the target to the substrate. These two issues are addressed in the following paragraphs.

4.1.1. Target-plasma interactions and target erosion rate

In a first approximation, the deposition rate in sputtering processes is proportional to the target erosion rate (Φ), i.e. the number of species ejected from the target per time and area unit. The erosion rate is, in turn, equal to

$$\Phi = j_i \times Y \quad (10)$$

where j_i is the number (current) of ions impinging onto the target per time and area unit and Y designates the sputtering yield, namely the number of particles sputtered per impinging ion. In conventional sputtering processes (e.g. dcMS) the ion target current consists mostly of Ar^+ species [13], i.e.

$$j_i^{\text{dcMS}} \approx j^{\text{Ar}^+} \quad (11)$$

which implies that the erosion rate is equal to

$$\Phi^{\text{dcMS}} \approx j^{\text{Ar}^+} \times Y^{\text{Ar}^+} \quad (12)$$

The total ion current is proportional to the average current applied to the target (I_{Tav}). The sputtering yield, for a given ion target

combination, exhibits a power-law dependence on the energy (E) of the impinging ions [115], i.e.

$$Y \propto E^m \quad (13)$$

with $m < 1$. The ion energy is, in turn, equal to

$$E = q \times eV_T \quad (14)$$

where V_T is the target voltage, q stands for the charge state of the impinging ion and e designates the elementary charge. Deposition at a constant average target power (P_{Tav}) implies that

$$P_{\text{Tav}} = I_{\text{Tav}} \times V_T = \text{const.} \quad (15)$$

It is known that the HPPMS discharges are driven by cathode potentials in the range of 400 to 2000 V [33,34,116], exceeding the target potentials commonly employed in dcMS (~300 V) [33,34]. This fact in combination with Eq. (15) means that the use of a constant average target power leads to lower I_{Tav} values in HPPMS. The lower I_{Tav} values are equivalent with a decrease of the flux of ions to the target and thus, of a decrease in the target erosion rate (Eq. (10)) [34]. This decrease cannot be compensated by the increase of the target voltage, due to the non-linear dependence of the sputtering yield on the ion energy [116], as demonstrated in Eq. (13). This argument implies that, when the target voltage is increased and the average power is maintained constant, a loss of deposition rate should be expected, irrespective of the deposition process used. Furthermore, the values of the relative HPPMS-to-dcMS deposition rates reported in the literature [25,70] are even lower than those which correspond to the sputtering process described by Eq. (12), i.e. sputtering of the target by Ar^+ ions. Thus, a different mechanism has to be invoked, in order to explain these findings. A number of early studies on the deposition rate in HPPMS [25,117] suggested that the high degree of ionization obtained with this technique leads to an increased probability for ionized sputtered species (M^+) to be re-directed towards the target and self-sputter resulting in a time-averaged ion current

$$j_i^{\text{HPPMS}} = j^{\text{Ar}^+} + j^{\text{M}^+}. \quad (16)$$

The presence of M^+ ions in the ion flux towards the target results in an erosion rate equal to [118],

$$\Phi^{\text{HPPMS}} = j^{\text{Ar}^+} \times Y^{\text{Ar}^+}(E) + j^{\text{M}^+} \times Y^{\text{M}^+}(E) - j^{\text{M}^+} \quad (17)$$

with $Y^{\text{M}^+}(E)$ being the energy dependent sputtering yield of M^+ ions (also referred to as self-sputtering yield). The term “ $-j^{\text{M}^+}$ ” on the right-hand side of Eq. (17) accounts for the self-sputtering and results in a decrease of the total number of sputtered species as compared to dcMS. The sputtering yield (Y^{Ar^+}) is for most metals higher or comparable to the self-sputtering yield (Y^{M^+}), as shown by the values calculated using the TRIM software [119] in Table 2. This further contributes to the decrease of Φ^{HPPMS} with respect to Φ^{dcMS} . Christie summed up these ideas [117] in a description of the pathways of ionized and neutral species from the target to the substrate and

Table 2
Sputtering (Y^{Ar^+}) and self-sputtering (Y^{M^+}) yield of common metal calculated using the TRIM freeware. The energy of the incident ions was set to 500 eV.

| Target | Y^{Ar^+} | Y^{M^+} |
|--------|-------------------|------------------|
| Ti | 0.634 | 0.519 |
| Cr | 1.407 | 1.154 |
| Cu | 2.443 | 2.046 |
| Al | 0.306 | 0.462 |
| Ta | 1.002 | 0.714 |
| C | 0.032 | 0.090 |

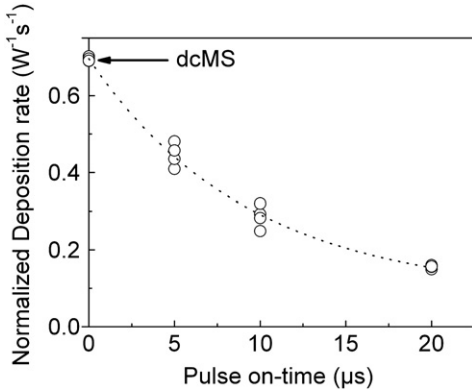


Fig. 20. Deposition rate (measured by a quartz crystal microbalance) of Ti films normalized to the average power applied to the target. The increase of the pulse on-time results in a decrease of the deposition rate. In all cases, rates lower than those achieved by dcMS (indicated by the solid arrow) are obtained. The dotted line is a guide to the eye (data taken from [70]).

derived an expression for the HPPMS-to-dcMS deposition rate ratio a_D as a function of the ionization degree of the sputtered material (β), the sputtering (by Ar^+ ions) and the self-sputtering yields, i.e.

$$a_D = \frac{1-\beta + \beta(1-\sigma)}{1 + \beta\sigma(Y^{Ar+} - Y^{M+})} \quad (18)$$

where σ is the fraction of ionized sputtered species which are confined in the target's vicinity and re-directed to the target for sputtering. According to Eq. (18), the HPPMS deposition rate decreases as the ionization of the sputtered material and/or the redirection of ionized sputtered species to the target are increased [117]. It is evident that the understanding of the mechanisms that determine the ionization and the re-direction of ionized sputtered species is of key importance in order to better clarify the deposition rate changes observed in HPPMS. In general, an increase of the fraction of ionized species can be obtained via an increase of the efficiency of the ionization process. In HPPMS the electron impact is the dominant ionization mechanism [120]. Thus, higher electron densities and energies, as well as longer interaction times of the sputtered species with the energetic electrons would lead to an increase of the ionization degree [120]. This can be, for instance, achieved by increasing the target voltage, the average and peak target

power (or current) during the HPPMS operation [33,34,38,65], as well as by increasing the pulse on-time [39,70]. In all these cases a decrease of the deposition rate has been demonstrated for a number of target materials [25,34,38,70,118,121], see e.g. Fig. 20. As explained in Section 3, the high values of peak target current are decisive for the plasma composition in the target's vicinity, since they result in high ionization degrees of the sputtered species and depletion of Ar gas in front of the target, i.e. gas rarefaction. Investigations of the plasma composition in a number of Ar-metal HPPMS discharges have demonstrated that the high ionization, the gas rarefaction, and the loss of the deposition rate are observed simultaneously [34,70]. The gas rarefaction signifies that less Ar is available for ionization during the pulse on-time, which contributes to the abundance of M^+ species in the target's vicinity and to the high re-direction probability [34,70]. In order to identify whether the rarefaction is a necessary condition for the loss of the deposition rate to occur, Alami et al. [34] studied the plasma composition and the deposition rate of Cr films grown by HPPMS and dcMS. In this study a constant average target current was used [34], which allows for an easy understanding of the underlying physics, since in a first approximation [34] the total ion target current remains constant at all deposition conditions. Thus, according to Eqs. (10)–(18), changes in the target erosion rate can be assigned to changes in the composition of the ion target current and the ion energy (i.e. target voltage) [34]. In Fig. 21 the deposition rate of Cr is plotted as a function of the peak target current density for two pulse on/off time configurations. It is seen that the increase of the pulse off-time from 950 to 2450 μs led to a higher peak target current density (I_{TpD}) and a decrease in the deposition rate. However, when the pulse on/off time configuration was held constant, the increase of the peak target current density up to a value of ~0.57 A cm⁻² resulted in HPPMS rates equal to the dcMS ones (dotted lines in Fig. 21). Above this value, and irrespective of the pulse on/off time configuration used, the HPPMS deposition rates deviated from the dcMS rates. It was shown in Ref. [34] that under these conditions ($I_{TpD} > 0.57 \text{ A cm}^{-2}$) the ionization of the sputtered material increased significantly, while rarefaction was observed (see Fig. 14(c) and (d)). Gas rarefaction was also observed below the characteristic value 0.57 A cm⁻² (Fig. 14(b)), where the ionization degree was lower than the ionization at I_{TpD} values above 0.57 A cm⁻² [34]. This implies that simultaneous high ionization and Ar rarefaction are necessary conditions for triggering the self-sputtering and loss of the deposition rate [34]. Based on Eqs. (12), (16) and (17) and using the constant average current approach Sarakinos et al. [118] derived the following expression for the HPPMS ($R^{HPPMS} d$) to the dcMS rate ratio($R^{dcMS} d$):

$$\frac{R^{HPPMS}}{R^{dcMS}} \propto f^{Ar+} \cdot \frac{Y^{Ar+}(E)}{Y^{Ar+}(E_0)} + f^{M+} \cdot \frac{(Y^{M+}(E)-1)}{Y^{Ar+}(E_0)} \quad (19)$$

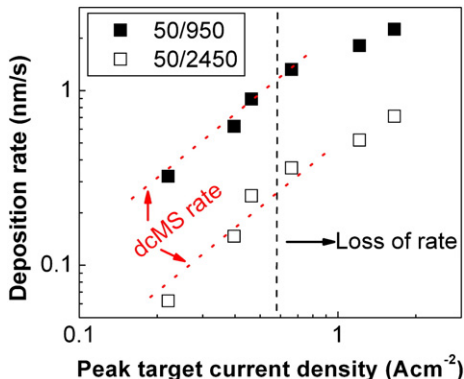


Fig. 21. Dependence of the deposition rate of HPPMS grown Cr films on the peak target current. The films have been deposited using pulse off-times (950 and 1450 μs) at a constant pulse on-time of 50 μs. The dotted straight lines represent the deposition rates obtained by dcMS at the average target current values which were used during the HPPMS experiments in order to achieve the peak target current density values indicated in the x-axis of the figure. The deposition rate deviates from the dcMS one at the well-defined peak target current density value of 0.57 A cm⁻² irrespective of the pulse on/off time configuration used (data taken from [34]).

In Eq. (19) f^{Ar+} and f^{M+} are the relative fractions of Ar^+ and target ions (M^+) in the target current. $Y^{Ar+}(E)$ and $Y^{M+}(E)$ are the sputtering and the self-sputtering yields as functions of the energy of the sputtering ions, while $Y^{Ar+}(E_0)$ is the sputtering yield at the reference dcMS conditions [118]. In order to quantify the dependence of the composition of the ion target current on the target material at the various deposition conditions, Eq. (19) was fitted to experimentally measured deposition rates for C, Cr, and Cu [118]. The analysis showed that in the case of C the current almost exclusively consisted of Ar^+ ions at all deposition conditions [118]. On the other hand, the results for Cr and Cu indicated a transition from an Ar^+ - to an M^+ -dominated current, when the peak target current was increased [118]. The absence of C^+ ions in the ion flux to the target calculated for C could be attributed to the lower sputtering yield (Table 2) and the lower ionization probability of this material [122–124], in comparison to Cr and Cu [122–124]. The lower sputtering yield results in lower fluxes of sputtered species, which in turn lead to a less pronounced

gas rarefaction [86], while the lower ionization probability contributes further to the relative reduction of the local C^+ population [118]. Owing to the above presented plasma characteristics the deposition rate for C films did not deviate from the dcMS one, while in the case of Cr and Cu the pronounced self-sputtering resulted in lower deposition rate when the average target power was used for comparison [118].

4.1.2. Transport of ionized sputtered species

In HPPMS the transport of ionized sputtered species from the target to the substrate has a significant influence on the magnitude of the deposition rate, due to the high fractions of ions in the flux of the sputtered material. In general, the trajectories and thus, the transport of sputtered particles are determined by the velocity angular distribution at the target and their collisions with gas atoms [2,115]. In addition, when the sputtered particles are charged, the presence of electric and/or magnetic fields can also affect their transport [30]. This is discussed in Section 3, where the azimuthal electron current above the race track in HPPMS exerts a tangential outward force on the ions [100]. Thus, part of the ions moves along off-normal, with respect to the target, directions resulting in a decrease of the net flux of material on substrates placed parallel to the target surface [101]. In order to enhance the ion transport along the target normal, a number of workers [38,103,104] employed experimental arrangements which enabled an increase of the electron density and energy in the bulk of the plasma and the substrate's vicinity. These arrangements included secondary coils behind the substrate [104] and strongly unbalanced magnetrons [38] and led to an increase of the deposition rate [38,104]. Others [44,73,74] superimposed an inductively coupled plasma (ICP) on the HPPMS plasma and observed that the ions reach the substrate in two successive waves; the first during the pulse on-time and the second in the post-discharge time (Fig. 22). Absorption and emission spectroscopy measurements revealed that the first wave consisted of Ar^+ ions, while the second one of Ti^+ ions [73]. The superposition of the ICP with various powers did not affect the first ionic wave, while it resulted in a faster transport of the second (Ti^+) wave, as shown Fig. 22. Konstantinidis et al. [73] suggested this to be the effect of the enhanced ambipolar diffusion due to the increase of the electron energy by the secondary plasma which was later verified experimentally by time-resolved Langmuir probe measurements performed by de Poucques et al. [74]. The correlation between the charge transport and the deposition rate was also described theoretically by Vlcek et al. [38] who expanded the formalism presented by Christie [117] and derived the following expression for the HPPMS-to-dcMS rate ratio

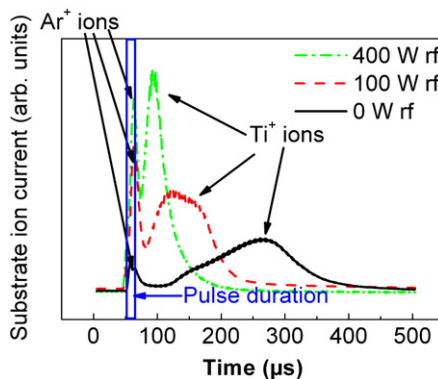


Fig. 22. Effect of the inductively couple plasma power on the substrate ion current in an $Ar-Ti$ HPPMS discharge. The increase of the power results in a faster transport of Ti^+ ions, while the Ar^+ species remain unaffected (data taken from [73]).

$$a_D,$$

$$a_D = \frac{(1-\beta)\left(1-\gamma + \gamma \frac{\xi_i}{\xi_n}\right) + \beta(1-\sigma)\frac{\xi_i}{\xi_n}}{1 + \beta\sigma(Y^{Ar^+} - Y^{M^+})} \quad (20)$$

In comparison to Eq. (9) the additional parameters included in Eq. (20) are the efficiency of the transport for neutral (ξ_n) and ionized (ξ_i) sputtered species and the probability of ionization for sputtered atoms (γ) in the bulk plasma [38]. Eq. (20) predicts an increase of the HPPMS rate when the efficiency of the ion transport (ξ_i) and the ionization of the sputtered atoms in the bulk plasma (γ) are increased [38].

4.2. Reactive HPPMS

The addition of a reactive gas into the sputtering atmosphere leads to target coverage, i.e. chemisorption [125] and/or implantation [126] of reactive gas species at the target surface and the sub-surface layers, respectively. Deposition from a fully covered target (referred to as the compound sputtering mode) allows for growth of stoichiometric compound films, i.e. compound films with sufficient incorporation of the reactive gas atoms [125]. At these conditions deposition rates lower than those obtained from an elemental (e.g. metallic) target are commonly achieved [125]. Growth of stoichiometric compound films with relatively high rates can be facilitated in the intermediate target coverage regime (referred to as transition zone) between the metallic and the compound mode [125]. In reactive dcMS the transition sputtering zone is frequently unstable, and a hysteresis in the process parameters is often observed [125]. This is particularly pronounced during reactive dcMS of metal oxides [127]. As a consequence, stoichiometric films can only be obtained in the compound sputtering mode [125], unless a feedback system for controlling the target coverage is employed [128].

Earlier studies on the reactive HPPMS of various metal oxides (TiO_2 , ZrO_2 , Ta_2O_5) revealed deposition rates ranging between 25% and 120% of rates achieved by dcMS, mid-frequency pulsed sputtering, and ac magnetron sputtering, as shown in Table 1. In these studies the obtained deposition rates were interpreted in light of the self-sputtering phenomenon [107,109]. More recently, systematic investigations of the reactive HPPMS of Al_2O_3 [129] and ZrO_2 [130] showed that the HPPMS process can exhibit a hysteresis free and stable transition zone at deposition conditions which in the case of dcMS result in hysteresis and unstable transition zone, as demonstrated for

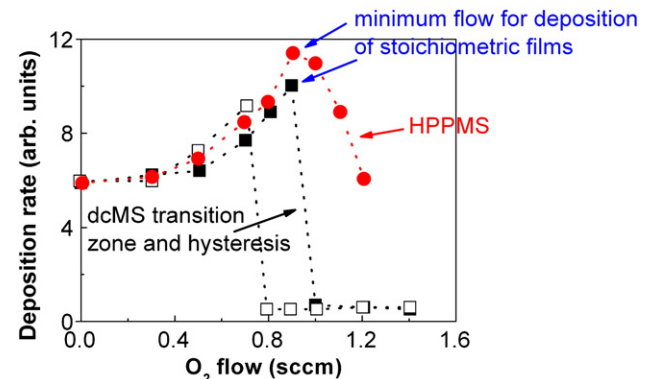


Fig. 23. Deposition rate during reactive deposition of Al_2O_3 by dcMS and HPPMS measured with a quartz crystal microbalance. The filled and hollow squares correspond to the dcMS rate for increasing and decreasing O_2 flow, respectively. It is seen that the dcMS process exhibits an unstable transition zone with pronounced hysteresis. On the contrary the HPPMS process (filled circles for both increasing and decreasing O_2 flow) is stable and hysteresis free. This behavior allows for a deposition rate similar to that obtained by dcMS (data taken from [129]).

the reactive deposition of Al_2O_3 in Fig. 23. The stabilization of the transition zone allows for deposition of stoichiometric films at a lower target coverage, when compared to the compound mode in dcMS [129,130], and has been shown to result in rates similar to [129] (Fig. 23) or up to two times higher [130] than the dcMS rates. Higher deposition rates have also been reported for ZnO films [46]. In this case the apparent growth rate determined by the film thickness was lower than that in dcMS. However the amount of the deposited material was the same [46] and the lower growth rate in HPPMS is understood to be the result of the densification of the film [46].

In general, the stability of the transition zone in reactive sputtering processes is determined by the competition between the formation and the removal (sputtering) of the compound from the target surface [125]. According to the formalism developed by Berg and Nyberg [125] the steady-state target coverage, ϑ_t , is equal to,

$$\frac{J_i Y_c \vartheta_t}{q} - a2F(1-\vartheta_t) = 0 \quad (21)$$

where J_i is the ion target current density, Y_c the compound sputtering yield, q the elementary charge, a the sticking coefficient of the reactive gas and F the flux of the reactive gas molecules towards the target [125]. Stabilization of the transition mode can be achieved, if for a certain nominal partial pressure/flow of the reactive gas the term $\frac{J_i Y_c \vartheta_t}{q}$ (removal of the compound) increases and/or the term " $a2F(1-\vartheta_t)$ " (formation of the compound) decreases. The pulsed character of the HPPMS discharge affects both terms in Eq. (21). The high peak currents (up to three orders of magnitude higher than the average values) result in a significantly higher instantaneous erosion rate during the pulse on-time, which may effectively clean the target surface and displace the oxidation onset at higher reactive gas flows [129]. In addition, the absence of plasma during the pulse off-time results in a limited activation of the reactive species [131]. Under these conditions relatively high levels of reactive gas exposure are necessary for the formation of the compound on the target surface, i.e. this mechanism leads to lower effective values of the sticking coefficient a in Eq. (21). Furthermore, as a result of the high target voltage in HPPMS [34] higher compound sputtering yields Y_c and as a consequence higher values of the compound erosion rate (normalized to the ion target current density) can be achieved [130]. However, a necessary condition for this to occur is that Ar^+ is a significant fraction of the ion target current [130], i.e. the effect of self-sputtering on the target erosion rate is low [130]. The latter is the case when relatively moderate values of peak target current are applied [34]. The high peak target current in HPPMS results in rarefaction of the neutral species in

the target's vicinity, as discussed in Section 3, which affects not only the Ar but also the reactive gas [130]. This is shown in Fig. 24 for the reactive HPPMS deposition of TiO_2 . During the pulse on-time the emission intensity of Ti^+ species increases, while that of Ar and O initially increases and then decreases. The rarefaction implies that the reactive species flux F lower than the value which corresponds to the nominal partial pressure of the reactive gas should be expected [130].

5. Growth of thin films by HPPMS

In magnetron sputtering techniques, variation of the deposition parameters allows for control of the energy transferred to the film forming species enabling the manipulation of the films properties [1,2]. Among the various ways used to provide energy to the growing film, bombardment by ionized species is widely employed [4,132]. Numerous studies have shown that during the film growth, the plasma–film interface is affected by the energy of the bombarding ions, their flux, their nature, and their angle of incidence [5,12]. These parameters determine the efficiency of the momentum transfer to the film atoms [133] and have been shown to have implications on the film microstructure [5] as well as on mechanical, optical, and electrical properties [4,134,135]. The results presented in Section 3 revealed that, by using HPPMS, high pulsed ion fluxes are made available at the substrate. The magnitude and the composition of these fluxes can be controlled by changing the process parameters, e.g. the peak target current, the pressure, the deposition angle, and the magnetic field strength. In the next paragraphs the effect of the energetic bombardment during HPPMS on the growth and the properties of elemental and compound films is reviewed.

5.1. HPPMS use for deposition on complex-shaped substrates

The deposition of homogeneous films on substrates of complex geometry is a requirement for many technological applications, such

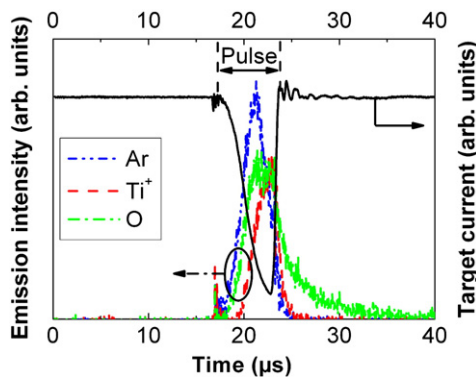


Fig. 24. Temporal evolution of the emission intensity of Ti^+ , Ar, and O species during the reactive deposition of TiO_2 by HPPMS. The Ti^+ intensity increases throughout the pulse on-time, while that of Ar and O increases during the first 5 μs of the pulse and then decreases indicating rarefaction (S. Konstantinidis, unpublished data).

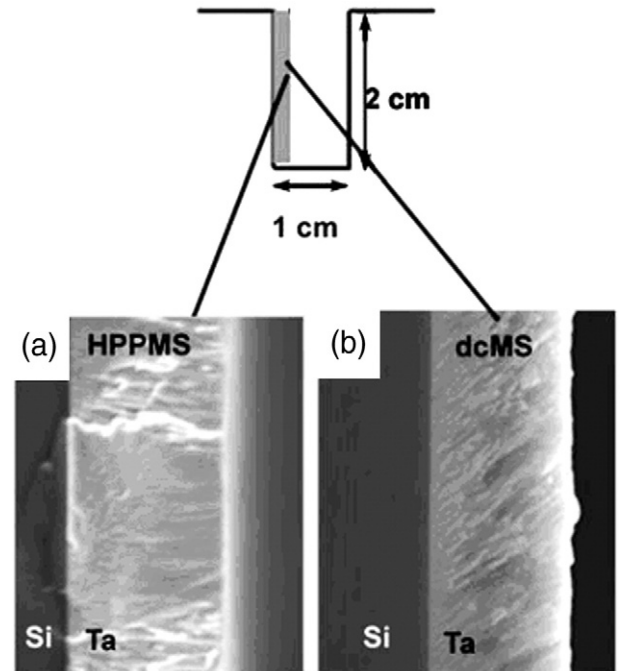


Fig. 25. Cross sectional SEM images of Ta films grown by (a) HPPMS and (b) dcMS on a silicon substrate clamped on the side of a trench with an area of 1 cm^2 and a depth of 2 cm. The HPPMS deposited film is dense with columns growing perpendicular to the Si/Ta interface. On the other hand, dcMS grown films exhibit a porous morphology with column tilted from the interface normal as a result of the atomic shadowing (reprinted from [138] after permission, American Institute of Physics © 2005).

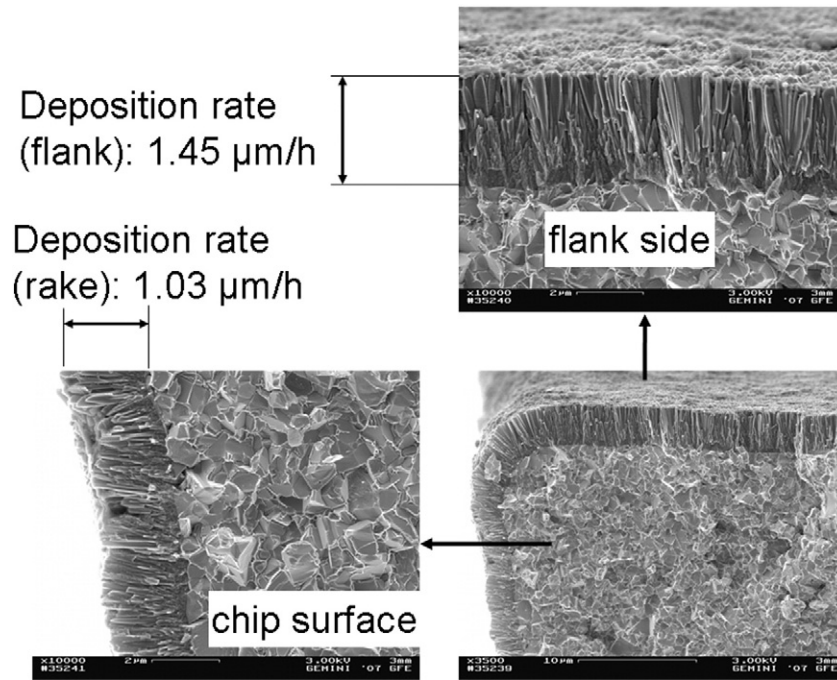


Fig. 26. Cross sectional SEM images of TiAlN coating deposited on the flank and the rake side of a cutting insert (reprinted from [105] after permission, Elsevier © 2009).

as metallization of sub-micrometer patterns in optical and semiconductor devices [112–114] and deposition of thick protective layers on forming tools and turbine blades [105,136,137]. In conventional sputtering techniques, such as dcMS, the sputtered material consists largely of neutral species. The trajectories of the neutral species are determined by the initial angular distribution of their velocities at the target and the gas-phase scattering [2,115] which result in a highly anisotropic deposition flux [132], and a faster deposition along the line of sight. Thus, substrate sites located along low flux directions are shadowed leading to inhomogeneous deposition, porosity, and poor coverage [113]. The microelectronics industry first recognized that a high degree of ionization of the deposited flux can be advantageous, as the energy and the trajectory of ions can easily be manipulated through the use of electric and magnetic fields. Different attempts to achieve this include the use of hollow cathodes [25], electron cyclotron resonance devices [25], inductively coupled rf generators [25] in conjunction with the magnetron discharge, as well as by employing filtered cathodic arc [113].

HPPMS provides an alternative approach to successfully deposit films on complex-shaped substrates. In Fig. 25, the cross-section SEM images of Ta films deposited both by dcMS and HPPMS on a negatively biased (-50 V) Si substrate clamped on the side of a trench with an area of 1 cm^2 and a depth of 2 cm are presented [138]. The SEM images were taken from a position at the middle of the trench as shown in the sketch in Fig. 25. The dcMS grown film exhibits a porous columnar structure with columns orientation tilted from the normal of the Ta/Si interface [138] (Fig. 25(b)), while the HPPMS films are dense with columns growing perpendicularly to the Ta/Si interface (Fig. 25(a)) [138]. These findings are consistent with the notion that dcMS is a line-of-sight deposition method giving rise to underdense films, due to atomic shadowing [132], and suggest that the HPPMS process can alleviate some of the problems related to this. Smaller features, such as holes of several tenths or hundreds of nm could therefore be successfully filled [31] or homogeneously coated [54], as demonstrated in Fig. 4 [31]. The beneficial use of HPPMS is further illustrated by the deposition of homogeneous hard nitride coatings on cutting inserts [105]. In Fig. 26 the cross-section SEM micrograph of a cutting insert coated by TiAlN deposited by HPPMS shows that

deposition rates of $1.45\text{ }\mu\text{m}/\text{h}$ and $1.03\text{ }\mu\text{m}/\text{h}$ are obtained on the flank (facing the target) and on the rake (perpendicular to the target) side of the substrate, respectively. For comparison, the dcMS and mid-frequency pulsed sputtering (not shown in Fig. 26) coated inserts exhibited flank side rates of 1.46 and $1.35\text{ }\mu\text{m}/\text{h}$, respectively, while the corresponding values for the rake side were $0.65\text{ }\mu\text{m}/\text{h}$ and $0.8\text{ }\mu\text{m}/\text{h}$.

5.2. Interface engineering by HPPMS

It is well established that the adhesion of a film on a substrate is one of the critical properties for its functionality and life-time. The quality of the surface where the film/substrate interface is formed is decisive for the adhesion [139]. In general, the exposure of a surface to the atmosphere leads to contamination and formation of oxide and organic layers [139]. These layers result in weak van-der-Waals forces between the film and the substrate and subsequently, to a poor film adhesion [139]. In order to enhance the adhesion, cleaning of the

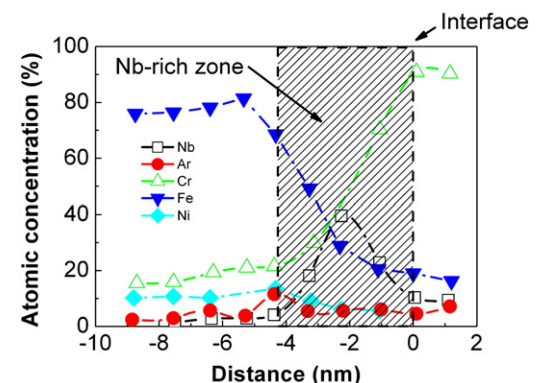


Fig. 27. Chemical composition of a steel-CrN/NbN interface etched by an Ar-Nb HPPMS discharge. Nb atoms are subplanted into the substrate over a thickness range of 5 nm (data taken from [139]).

surface prior to the film deposition is performed. In the industrial practice, Ar^+ ions are used for this purpose and the process is referred to as ion etching. The Ar^+ ions are generated from Ar gas using external ionization sources (e.g. hollow cathodes and electron guns) which are mounted at the deposition chamber [105,136,140]. Subsequently, the Ar^+ ions are extracted and accelerated towards the substrate by applying a negative bias voltage ranging from 300 V up to 1 kV. Alternatively metal ions can be used for etching the substrate [24,141,142]. This has been, for instance, demonstrated for steel and WC substrates etched using cathodic arc evaporation [24], which is a technique that provides nearly a 100% ionized metal discharge [25]. However, the major drawback of cathodic arc evaporation is the existence of macroparticles which may deteriorate the quality of the interface. Ehiasarian et al. [139,143,144] have demonstrated that the high ion metal fluxes available in the HPPMS discharge can also be utilized for the engineering of the interface in a number of monolithic and multilayer films. For example, they found that a CrN/NbN film deposited on steel substrates etched using HPPMS (pretreatment by Nb^+ ions at a substrate bias voltage of -1000 V) exhibited a scratch test critical load (L_c) of 56 N which was higher than the values of 25 N obtained for films deposited on substrates etched by dcMS plasma (substrate bias voltage of -1000 V at an Ar pressure of 0.8 Pa), which exhibit a significantly lower ionization degree for both Ar^+ and metal ions [139]. It should be also pointed out here that the L_c values achieved on HPPMS etched substrates are comparable to those for films grown on substrates cleaned using high fluxes of Ar^+ ions generated by an external ionization source [140]. This fact indicates that HPPMS could be employed as an alternative process to improve the quality of the film/substrate interface and enhance the film adhesion, when no external source for increasing the Ar ionization is available. When HPPMS is used for substrate etching, the bombarding metal ions are subplanted into the substrate forming a film/substrate interface with thicknesses ranging between 5 and 15 nm [139,143]. This is, for instance, the case for a multilayer CrN/NbN coatings deposited on steel substrate etched using an Ar–Nb HPPMS discharge [139] (Fig. 27). It is seen that Nb populates the interface at a depth of up to ~ 5 nm with a maximum atomic concentration of $\sim 40\%$ at a depth of ~ 2 nm, which leads to local epitaxial growth of individual film grains on substrate grains [139].

5.3. The effect of HPPMS on the film microstructure

Polycrystalline films grown by PVD techniques exhibit a variety of microstructures with respect to the size, the morphology, and the relative orientation of the crystallites [5,6]. These features have, for instance, implications on the mechanical strength [145] and the electrical conductivity [134,135,146] of the film. The microstructure is determined primarily by surface and bulk diffusion processes [5,6] which are controlled by the deposition temperature (T_s) and the

concentration of impurities that act as inhibitors for the crystal growth. The effect of the temperature can be quantified using the so-called homologous temperature $\frac{T_s}{T_m}$ (T_m is the melting temperature of the deposited material) and the obtained microstructural features can be classified according to the structural zone models (SZM) [7–10]. A qualitative SZM that describes the sputter deposition of metallic films is shown schematically in Fig. 28. Zones I, T and II refer to an impurity-free growth. In Zone I (typically for $\frac{T_s}{T_m}$ values below 0.2), due to the limited surface diffusion, the lateral size of the grains is determined by the nucleation density. As a consequence the film consists of uninterrupted fibrous columns and exhibits porous and rough morphologies and a random texture [5,6]. In zone T (typically in the $\frac{T_s}{T_m}$ range 0.2 to 0.4) the surface diffusion has considerable influence on the growth. This fact leads to competitive growth at the interface (manifested by V-shaped grains), since grains with different crystallographic orientations provide different diffusion coefficients and therefore different residence times for the adatoms. At larger film thicknesses faster growing grains overwhelm slower ones giving rise to a columnar dense morphology, smoother surfaces and strong texture [5,6]. At higher temperatures ($\frac{T_s}{T_m} > 0.4$; Zone II) bulk diffusion becomes significant giving rise to a dense columnar microstructure which is retained from the interface to the film surface [5,6]. Zone III is

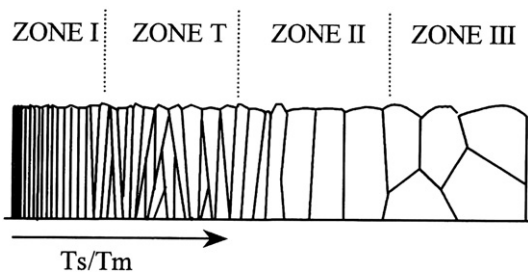


Fig. 28. Qualitative schematic representation of the structural zone model for sputter deposition of metallic films (reprinted from [6] after permission, Elsevier © 1998). Zones I, T and II refer to impurity-free deposition, while zone III describes high temperature growth under the presence of low concentration of impurities.

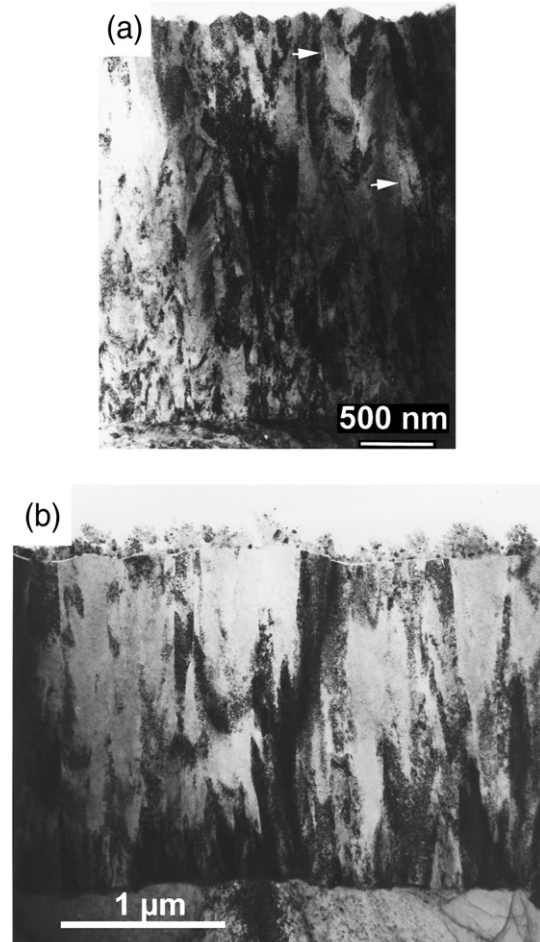


Fig. 29. Cross-section TEM images of CrN films deposited by (a) dcMS and (b) HPPMS on high speed steel discs. The dcMS grown film exhibits an underdense columnar structure ending to a rough surface. The films deposited by HPPMS exhibit a dense microstructure, the columnar growth is suppressed and renucleation is observed (reprinted from [150] after permission, Elsevier © 2004).

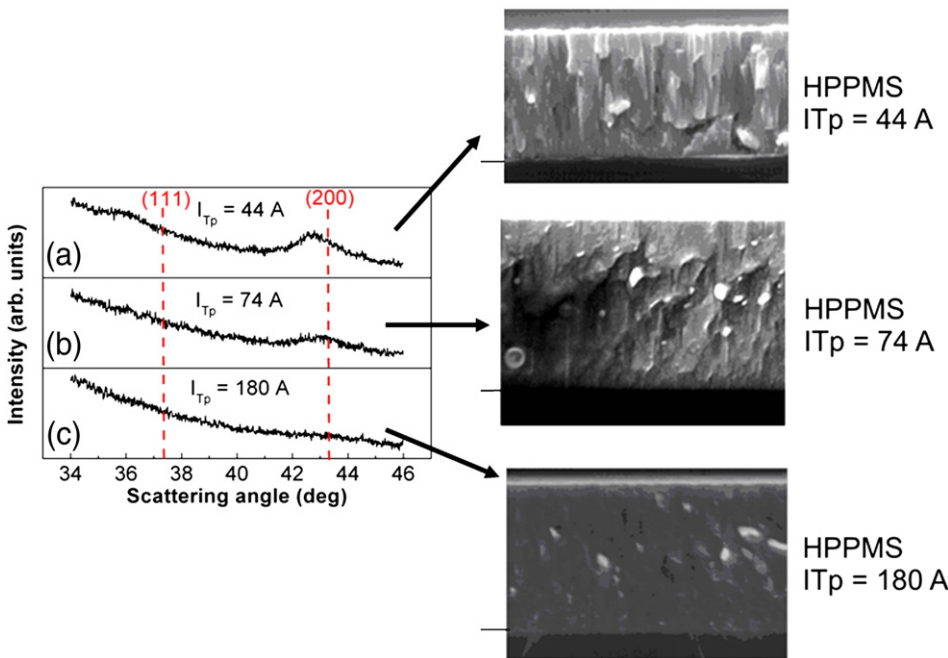


Fig. 30. Cross-sectional SEM images and X-ray diffraction patterns of CrN films deposited on Si by HPPMS at a peak target current of (a) 44 A, (b) 74 A and (c) 180 A. The increase of the peak target current results in a transition of a dense polycrystalline morphology to a nanocrystalline featureless one. The vertical dashed lines in the X-ray diffraction pattern indicate the position of the (111) and (200) peaks in the unstrained bulk CrN (data taken from [149]).

characterized by equi-axed three-dimensional (globular) grains and it is observed at temperatures higher than those of Zone II. However, this growth mode can only occur when impurities with low concentration (<0.5%) are present during the film growth and can be explained on the basis of the periodic interruption of the crystal growth and renucleation caused by the impurities [5,6,147]. Increase of the impurity concentration results in globular microstructure at temperatures lower than those corresponding to Zone III [147].

The simultaneous use of low flux ion bombardment (in the range of mA cm^{-2} which is typical for conventional sputtering processes like dcMS) allows for the transitions between the structural zones to occur at lower temperatures [7,9] and for the morphological features predicted by the SZM's to remain valid [7,9]. On the contrary, growth of thin films during HPPMS is characterized by the high ion flux during the pulse on-time (up to several hundreds of mA cm^{-2}), as was shown in Section 3. Observations of the morphology of films grown by this technique have shown that the SZM in its classical form is no longer valid [54,143,148–150]. An example is given in Fig. 29 where cross-sectional TEM images of CrN films grown by HPPMS and dcMS under otherwise the same conditions are shown [150]. In contrast to the underdense columnar morphology and high surface roughness obtained by dcMS (Fig. 29(a)), the use of HPPMS resulted in film densification, surface smoothening and suppression of the columnar structure, as shown in Fig. 29(b). In addition, some columns grew on the top of existing columns, i.e. renucleation is observed [150]. As mentioned above, in films grown under low flux ion irradiation the renucleation occurs when the individual grain growth is inhibited by contaminants [6]. The renucleation can be enhanced when the plasma ionization and thus the substrate ion current are increased, e.g. by increasing the peak target current [34,149]. This can facilitate the transition from a dense polycrystalline to a featureless/nanocrystalline structure [149], (Fig. 30) which resembles the microstructure of Zone III in Fig. 28. It is therefore evident that the low-energy high-flux ion irradiation during HPPMS [149] can be used in order to overcome the characteristically underdense and rough microstructures and obtain morphologies unique for low temperature deposition [149]. This in turn, allows deposition of films with higher hardness

[54,148,150], lower friction coefficient [143,148], and improved scratch and wear as well as corrosion resistance [148,150], as compared to films deposited by dcMS. Beside the changes in the film morphology, HPPMS affects also the texture of metal nitride films. For instance, HPPMS deposited CrN films were found to exhibit a (200) preferred growth orientation, in contrast to the (111) orientation observed for dcMS films [148]. This is consistent with the notion that the preferred orientation of transition metal nitride films with the rocksalt structure (e.g. TiN, CrN, etc.) can change from (111) to (200) when a more intense energetic bombardment is provided [151,152]. The energetic bombardment has been shown to enhance the surface diffusion allowing for the adatoms to be accommodated in the (200) planes which exhibit a lower surface free energy than that of the (111) planes [151,152]. A number of workers also investigated the effect of HPPMS on the growth of oxides and found that using this technique it is possible to control the texture of metal oxide films, such as ZnO which is a material used as a transparent conducting oxide [153]. The use of HPPMS allowed for deposition of ZnO films with an enhanced (002) texture compared to dcMS, a fact that resulted in a higher electrical conductivity [154].

5.4. Phase composition tailoring of films deposited using HPPMS

The phase composition of films is crucial for their mechanical, electrical, and optical performance. In sputtering processes relatively low growth temperatures and high deposition rates result in a limited mobility of the film forming species [2,3]. This induces kinetic limitations in the growth process and results in non-equilibrium growth [2,3]. Thus, the variation of both thermodynamic and kinetic conditions during deposition enables tailoring of the phase composition. Numerous studies have demonstrated that energetic ions can be used for this purpose, since they can trigger surface and bulk diffusion processes [2,3], induce changes in the film structure, [155] and cause generation of internal stresses [19,20,22,23]. The high fluxes of ionized material available in HPPMS have been found to allow for control of the phase formation in both elemental and compound films. For instance, HPPMS can be used to deposit carbon films with high fractions of

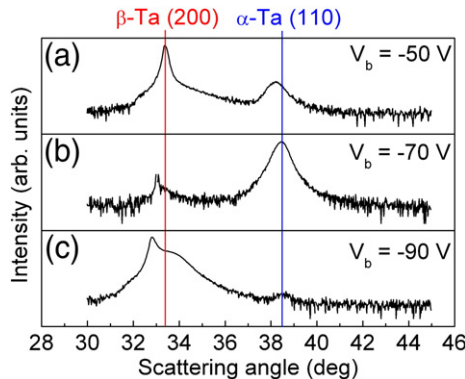


Fig. 31. X-ray diffraction patterns of Ta films deposited on Si substrates by HPPMS on negatively biased substrates at values of (a) 50, (b) 70 and (c) 90 V. The bcc α -Ta phase is obtained at 70 V as a result of the bombardment induced compressive stresses. The vertical dotted lines indicate the position of the β -Ta (200) and α -Ta (110) peaks (data taken from [110]).

diamond-like bonds, a feature that results in films with enhanced mechanical and tribological performance [17]. In order to obtain a high fraction of diamond-like bonds, bombarding energies that lead to ion subplantation and generation of internal compressive stresses are required [17,18]. Bugaev et al. [66] employed HPPMS for the deposition of carbon. Raman spectroscopy measurements revealed that the films contained a fraction of sp^3 (i.e. diamond-like) hybridized C atoms in the order of 50%–60% [66], which is higher than the typical sp^3 fraction of ~30% obtained from conventional sputtering techniques [17]. Although the ionization degree of C in HPPMS has been estimated to be in the order of 4.5% [111], these values of sp^3 content are not much lower than those obtained by techniques with a much higher degree of ionization like arc evaporation and pulse laser deposition [17]. The internal stresses and their effect on the phase formation can better be controlled when sputtered atoms of a target material that exhibits a higher degree of ionization are used. This is the case for Ta [110], a metal that exhibits ionization degrees of up to 70% in HPPMS [25]. Ta is particularly interesting for such an investigation because it forms both a low resistivity bcc crystal structure also known as the α phase at elevated temperatures and a metastable high resistivity tetragonal phase (β -Ta) at room temperatures [156,157]. The abundance of Ta^+ ions in the deposition flux during the HPPMS

deposition of Ta films implies a more efficient momentum transfer to the growing surface [12,110]. This is in contrast to the growth by dcMS where the majority of the ion flux consists of the much lighter Ar^+ ions [13]. HPPMS provides thus tools for better influencing the internal stresses of the growing Ta films and accordingly the possibility to deposit α -Ta films at room temperature (Fig. 31) [110].

In HPPMS discharges part of the ions moves along off-normal, with respect to the target, directions [101] (see Section 3). This abnormal ion transport results in differences in the flux, the energy, and the composition of the deposited and bombarding species as functions of the deposition angle. Substrates placed perpendicularly to the target surface are subjected to deposition fluxes with ion-to-neutral ratios higher than those on parallel oriented substrates [138]. In addition, the energies of the ionized species impinging on perpendicularly oriented substrates are, on average, lower than those along the target normal [101]. Another implication of the high ion-to-neutral ratios is that, in the case of compound targets, the composition of the material flux along off-normal directions is largely determined by the ionization fraction of the target's constituent elements [158]. This composition is different than that along directions close to the target normal which is also influenced by the angular distribution of the neutral species. The effect of the deposition angle on the phase composition has been studied for the ternary system Ti–Si–C [158]. This combination of elements is technologically interesting, since it can allow for the formation of the so-called MAX phases which exhibit an attractive combination of metallic and ceramic properties [159]. Regarding the composition of the deposited material, light elements like C are favored at the expense of heavier element, such as Ti and Si along the target normal [160]. On the other hand, substrates placed at an angle of 90° with respect to the target experience a lower flux of C, due to the lower ionization degree of C compared to Ti and Si [158]. In Fig. 32 the X-ray diffraction patterns of Ti–Si–C films grown from a Ti_2SiC_3 target employing HPPMS are presented. The TiC phase is the main constituent, for films grown on substrates parallel to the target surface (Fig. 32(a)). At

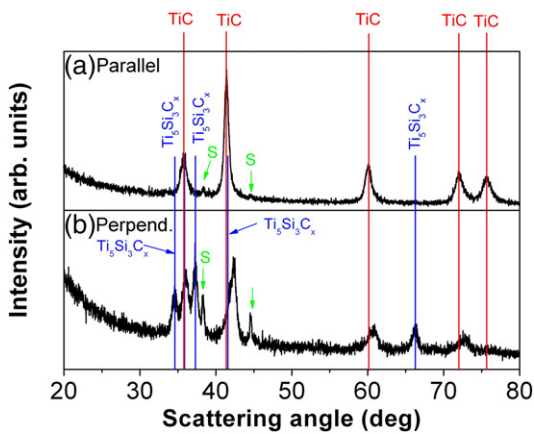


Fig. 32. X-ray diffraction patterns of Ti–Si–C films deposited on MgO (111) substrates by HPPMS on substrates oriented (a) parallel and (b) perpendicularly with respect to the target surface. The hollow circles and filled squares indicate the position of the peaks in bulk TiC_x and $Ti_5Si_3C_x$ phase, respectively (data taken from [158]).

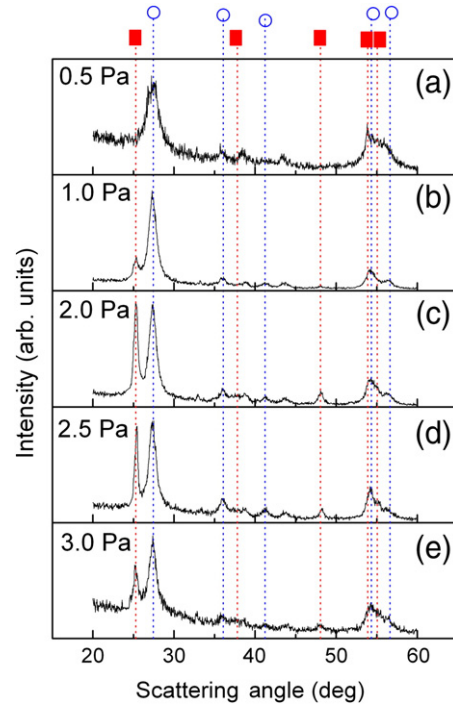


Fig. 33. X-ray diffraction patterns of TiO_2 films grown on Si substrates by HPPMS at a pressure of (a) 0.5 Pa, (b) 1, (c) 2, (d) 2.5 and (e) 3 Pa. The increase of pressure promotes the formation of the anatase at the expense of the rutile phase. The hollow circles and filled squares indicate the position of the peaks in bulk and unstrained rutile and anatase TiO_2 , respectively (data taken from [166]).

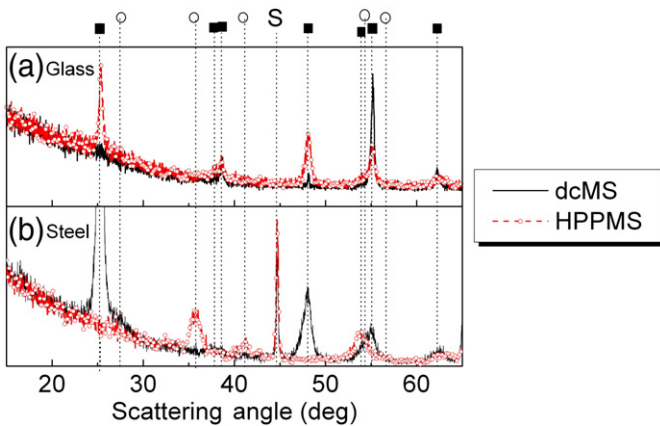


Fig. 34. X-ray diffraction patterns of TiO₂ films deposited by dcMS (solid lines) and HPPMS (hollow circles) on (a) glass and (b) steel substrates. A bipolar bias voltage of 50 V is applied to the steel substrate. The use of steel substrate enables the growth of the rutile phase when HPPMS is employed. The hollow circles and filled squares indicate the position of the peaks in bulk and unstrained rutile and anatase TiO₂, respectively. "S" indicates reflections that originate from the substrate (data taken from [45]).

deposition angle of 90° Nowotny's Ti₅Si₃C_x MAX phase is also formed, as shown Fig. 32(b). Alternatively to the multi-element targets, compound films can be deposited from elemental targets when a reactive gas is added in the sputtering atmosphere. This leads to the changes in the composition of the target (target coverage), as explained in Section 4.2. When O₂ is used as a reactive gas, the oxidized target surface is the source for the generation of negatively charged oxygen ions [161]. These ions are accelerated in the cathode sheath by the negative target potential towards the substrate [162] and it has been shown to have implications on the structure formation and the phase composition of reactively sputtered metal oxide films [163]. In HPPMS target voltages higher than those in dcMS are commonly observed, as shown in the previous sections. This implies that metal oxide films deposited by HPPMS do not only experience the high-flux low-energy bombardment by ionized sputtered species but they are also irradiated by O⁻ species with energies higher than those during dcMS.

The influence of low and high energy bombardment on the phase formation of HPPMS deposited metal oxides can be unraveled using TiO₂. In general, TiO₂ films can grow in an amorphous and in two tetragonal crystalline structures; the rutile and the anatase phases

[164]. Deposition and/or annealing at high temperatures (700–900 °C) have been reported to lead to the formation of the rutile phase [164]. The anatase phase is generally obtained at lower temperatures [164], while deposition at room temperature often leads to the formation of amorphous films [164]. In addition, the energetic bombardment by positively charged ions (facilitated by applying a negative bias voltage on the substrate) can promote the crystallization of TiO₂ films at room temperature [165]. When HPPMS is employed, the rutile phase can be achieved even at room temperature and the increase of the flux of energetic species towards the growing films favors the formation of the rutile at the expense of the anatase phase [45,166–168]. This can be, for instance, achieved by increasing the peak target current [168] or decreasing the working pressure during deposition (Fig. 33) [166,167]. It is also worth pointing out that the high fluxes of ionized species available during HPPMS have a more pronounced effect on the phase formation of TiO₂ films when conductive substrates are used [45], as shown in Fig. 34. Deposition on glass substrates leads to the growth of anatase films when both HPPMS and dcMS are used. On the other hand, deposition on steel substrates using HPPMS results in rutile films, while dcMS leads to the formation of anatase. In cases described above negative O⁻ ions coincide with positively charged ones in the bombarding flux. The trajectory of the O⁻ ions, when targets with no pronounced erosion track are used, is largely directional and perpendicular to the target surface [169]. Therefore, substrates placed perpendicular to the target surface will encounter a significantly suppressed O⁻ flux, as compared to parallel oriented substrates, as well as high positive ion-to-neutral ratios (see Section 3). The effect of the substrate orientation on the phase composition is shown in Fig. 35. Deposition on substrates facing the target leads to the growth of rutile-rich films (Fig. 35(a)) [166]. The deposition on the inclined substrates (Fig. 35(b)) also results in rutile films with a morphology that consists of crystallites embedded in an amorphous matrix [166].

6. Towards the industrialization of HPPMS

The present review coincides with the 10th HPPMS anniversary, and follows the review work by Helmersson et al. from 2006 [25]. It also comes in a time when the industrial interest for the HPPMS technique is growing, which is manifested by the increasing involvement of the industrial actors in the field. Therefore it might be predicted that in the coming few years we will witness new and innovative products based on the HPPMS technique. Since its emergence, research groups have investigated the HPPMS technique's relevance for industrial use, and showed the potentials of HPPMS to provide new means for alleviating some of the inherent problems related to conventional PVD approaches. However, these new advances have brought with them new challenges for the understanding of the underlying science and technology. In the present section, the attempts made to industrialize the HPPMS technique are reviewed and the challenges facing such a process are discussed.

6.1. Examples of industrially relevant coatings by HPPMS

The depositions of Transparent Conducting Oxides (TCOs) such aluminium-doped zinc (ZnO:Al) oxide and Indium Tin Oxide (ITO) have been performed by HPPMS, showing the positive effect of high-flux ion bombardment on the electrical conductivity and the surface smoothness of these coatings [154]. The benefit of using HPPMS lies in the fact that the substrate temperature during the deposition process is kept low which opens for new applications of the TCO materials. This example shows that HPPMS can serve as an elegant approach to overcome the shortcomings of conventionally used techniques. Another example for this are the studies performed on the deposition of α -Al₂O₃ films by HPPMS at low temperatures (650 °C) [170]. α -Al₂O₃ is commonly deposited by CVD at temperatures of about 1000 °C [171], while the temperature limit for the growth of α -Al₂O₃

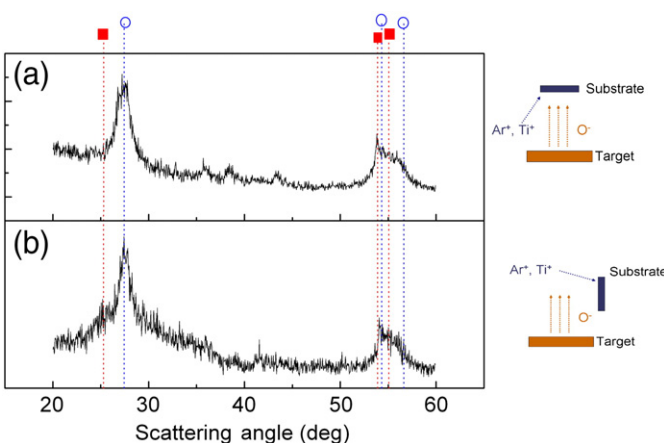


Fig. 35. X-ray diffraction patterns of TiO₂ films grown on Si substrates by HPPMS at a pressure of 0.5 Pa on substrates placed (a) parallel and (b) perpendicular to the target surface. The hollow circles and filled squares indicate the position of the peaks in bulk and unstrained rutile and anatase TiO₂, respectively (data taken from [166]).

by conventional pulsed magnetron sputtering is 760 °C [172]. Other examples include the deposition of functional nitride, oxide or metallic coatings, as detailed in Section 5.

6.2. Up-scaling of the HPPMS process

The examples demonstrated in the previous paragraph illustrate the potential products and applications of the HPPMS technique, but stay short of evaluating the technical complication linked to up-scaling and large volume production. Up-scaling entails understanding of the deposition process changes as a result of increasing the size of the deposition chamber and/or the load to be coated. This also means that the used power supplies should have the capability to provide the same plasma conditions as in the smaller laboratory scale. Examples of the challenges met by such a process are problems related to arcing of the target, which in most applications are unwanted effects. Other challenges manifest themselves in the difficulties experienced during the biasing of the substrate caused by the high peak ion currents. The new industrial interest in the HPPMS technique has, therefore, motivated the further development of the target and bias power supplies in order to meet the needs of large scale applications, as demonstrated in Section 2. The difficulties encountered in the up-scaling of processes are further enhanced when reactive depositions, especially of oxides, are performed. During reactive sputtering, the target to chamber surface ratio is of utmost importance for the stability of the deposition process. The up-scaling of the reactive process presents therefore added challenges to the process engineers and should be studied carefully before implementation. With respect to the deposition of oxides, it has been shown in laboratory scale experiments that with HPPMS, it is possible to smoothen the transition between the metal and the poisoned regimes and/or to eliminate the hysteresis phenomenon. This allowed for working in the transition zone without the struggle of a feedback control loop between the plasma monitoring system and the mass flow controllers. Moreover, in the case of zirconia, the deposition of the oxide compound was obtained while working on the edge of the transition zone resulting in a higher deposition rate with respect to dcMS. However, the benefits of reactive HPPMS in large scale industrial systems have not been yet proven and relevant deposition processes still need to be investigated.

6.3. Positioning HPPMS in the coating and components market

Industrial implementation of new technologies brings with it the added considerations of the cost effect, such as cost of power supplies, chamber modifications, operator training, and target materials. One of the main attractions of using HPPMS at an industrial scale is its ease of use. Simply by changing the conventional power supply into an HPPMS supply, new parameters are provided for the operator to influence the deposition process as explained throughout this review. Another attraction is the better target utilization and more homogeneous film thickness, which is especially important when the target price is very high [173]. It is important, however, to demonstrate the benefits of HPPMS in the context of the existing PVD techniques. Nowadays, arc evaporation and magnetron sputtering are well established in the cutting tool and component market. Nevertheless, in a number of applications, these conventional approaches fail to meet end-users' requirements. This is especially true for some applications where depositions are performed at low substrate temperatures or on complex-shaped substrates. In the present review HPPMS has been shown to be an attractive alternative, and should therefore be seen as a complementary technique that broadens the range of applications and coating designs, but also a technique that provides means to enhance the quality and performance of already existing coatings.

Acknowledgements

The authors would like to gratefully acknowledge Mr. Daniel Lundin (Linköping University, Sweden) for the discussions and his comments on Section 3 and Prof. Peter Barna (Research Institute for Technical Physics of Hungarian Academy of Sciences, Hungary) for his comments on Fig. 28. Prof. Ulf Helmersson (Linköping University, Sweden) and Dr. Denis Music (RWTH Aachen University, Germany) are also gratefully acknowledged for their comments on the manuscript. One of the authors (S.K) would like to acknowledge the Belgian National Fund for Scientific Research (FNRS) and the Interuniversity Attraction Poles Programme of the Belgian Science Policy (Project "PSI: Fundamentals of Plasma Surface Interactions") for the financial support.

References

- [1] D.M. Mattox, Handbook of Physical Vapor Deposition (PVD) Processing, Noyes Publications, Westwood, 1998.
- [2] M. Ohring, The Material Science of Thin Films, Academic Press, San Diego, 1992.
- [3] T. Michely, J. Krug, Islands Mountains and Atoms, Springer, Berlin, 2004.
- [4] O. Auciello, R. Kelly, Ion Bombardment Modification of Surfaces: Fundamentals and Applications, Elsevier Science Ltd, Amsterdam, 1984.
- [5] I. Petrov, P.B. Barna, L. Hultman, J.E. Greene, *J. Vac. Sci. Technol. A* 21 (2003) S117.
- [6] P.B. Barna, M. Adamik, *Thin Solid Films* 317 (1998) 27.
- [7] R. Messier, A.P. Giri, A.R. Joy, *J. Vac. Sci. Technol. A* 2 (1984) 500.
- [8] B.A. Mochan, A.V. Demchishin, *Phys. Met. Metallogr.* 28 (1969) 83.
- [9] J.A. Thornton, *Annu. Rev. Mater. Sci.* 7 (1977) 239.
- [10] C.R.M. Grovenor, H.T.G. Hentzell, D.A. Smith, *Acta Metall.* 32 (1984) 773.
- [11] J.S. Colligon, *J. Vac. Sci. Technol. A* 13 (1995) 1649.
- [12] J. Dalla Torre, G.H. Gilmer, D.L. Windt, R. Kalyanaraman, F.H. Baumann, P.L. O'Sullivan, J. Sapjeta, T. Díaz de la Rubia, M. Djafari Rouhani, *J. Appl. Phys.* 94 (2003) 263.
- [13] C. Christou, Z.H. Barber, *J. Vac. Sci. Technol. A* 18 (2000) 2897.
- [14] P.J. Kelly, R.D. Arnell, *Vacuum* 56 (2000) 159.
- [15] A. Ricard, C. Nouvelon, S. Konstantinidis, J.P. Dauchot, M. Wautelet, M. Hecq, *J. Vac. Sci. Technol. A* 20 (2002) 1488.
- [16] S. Konstantinidis, A. Ricard, M. Ganciu, J.P. Dauchot, C. Ranea, M. Hecq, *J. Appl. Phys.* 95 (2004) 2900.
- [17] J. Robertson, *Mater. Sci. Eng. R* 37 (2002) 129.
- [18] Y. Lifshitz, S.R. Kasi, J.W. Rabalais, *Phys. Rev. Lett.* 62 (1989) 1290.
- [19] G.C.A.M. Janssen, J.D. Kamminga, *Appl. Phys. Lett.* 85 (2004) 3086.
- [20] Y. Pauleau, *Vacuum* 61 (2001) 175.
- [21] R. Koch, *J. Phys. C: Condens. Matter.* 6 (1994) 9519.
- [22] H. Windischmann, *Crit. Rev. Solid State Mater. Sci.* 17 (1992) 547.
- [23] C.A. Davis, *Thin Solid Films* 226 (1993) 30.
- [24] P. Hovsepian, *Arch. Metall.* 33 (1988).
- [25] U. Helmersson, M. Lattemann, J. Bohlmark, A.P. Ehiasharian, J.T. Gudmundsson, *Thin Solid Films* 513 (2006) 1.
- [26] H.R. Kaufman, *J. Vac. Sci. Technol. A* 15 (1978) 272.
- [27] D.V. Mozgrin, I.K. Fetisov, G.V. Khodachenko, *Plasma Phys. Rep.* 21 (1995) 401.
- [28] S.P. Bugaev, N.N. Koval, N.S. Sochugov, A.N. Zakharov, *XVIIth International on Discharges and Electrical Insulation in Vacuum*, 1996, p. 1074.
- [29] I.K. Fetisov, A.A. Filippov, G.V. Khodachenko, D.V. Mozgrin, A.A. Pisarev, *Vacuum* 53 (1999) 133.
- [30] B. Chapman, *Glow Discharge Processes*, John Wiley & Sons, 1981.
- [31] V. Kouznetsov, K. Macák, J.M. Schneider, U. Helmersson, I. Petrov, *Surf. Coat. Technol.* 122 (1999) 290.
- [32] J.A. Thornton, *J. Vac. Sci. Technol. A* 15 (1978) 171.
- [33] A.P. Ehiasharian, R. New, W.-D. Münz, L. Hultman, U. Helmersson, V. Kouznetsov, *Vacuum* 65 (2002) 147.
- [34] J. Alami, K. Sarakinos, G. Mark, M. Wuttig, *Appl. Phys. Lett.* 89 (2006) 154104.
- [35] J.T. Gudmundsson, J. Alami, U. Helmersson, *Surf. Coat. Technol.* 161 (2002) 249.
- [36] J. Alami, PhD Thesis, Linköping University, Linköping, Sweden, 2005.
- [37] K. Sarakinos, PhD Thesis, RWTH Aachen University, Aachen, Germany, 2008.
- [38] J. Vlcek, P. Kudlacek, K. Burcalova, J. Musil, *J. Vac. Sci. Technol. A* 25 (2007) 42.
- [39] A. Anders, J. Andersson, A.P. Ehiasharian, *J. Appl. Phys.* 102 (2007) 113303.
- [40] J. Musil, J. Lestina, J. Vlcek, T. Tolg, *J. Vac. Sci. Technol. A* 19 (2001) 420.
- [41] I.I. Aksenov, V.A. Belous, V.G. Padalka, *Instrum. Exp. Tech.* 21 (1978) 1416.
- [42] H. Takikawa, H. Tanoue, *IEEE Trans. Plasma Sci.* 35 (2007) 992.
- [43] D.J. Christie, F. Tomasel, W.D. Sproul, D.C. Carter, *J. Vac. Sci. Technol. A* 22 (2004) 1415.
- [44] M. Ganciu, S. Konstantinidis, Y. Paint, J.P. Dauchot, M. Hecq, L. de Poucques, P. Vasina, M. Mesko, J.-C. Imbert, J. Bretagne, M. Touzeau, *J. Opt. Adv. Mat.* 7 (2005) 2481.
- [45] S. Konstantinidis, J.P. Dauchot, M. Hecq, *Thin Solid Films* 515 (2006) 1182.
- [46] S. Konstantinidis, A. Hemberg, J.P. Dauchot, M. Hecq, *J. Vac. Sci. Technol. B* 25 (2007) L19.
- [47] S. Konstantinidis, PhD Thesis, Université de Mons - Hainaut, Mons, Belgium, 2004.
- [48] P. Vasina, M. Mesko, J.-C. Imbert, M. Ganciu, C. Boisse-Laporte, L. de Poucques, M. Touzeau, D. Pagnon, J. Bretagne, *Plasma Sources Sci. Technol.* 16 (2007) 501.
- [49] A. Anders, G.Y. Yushkov, *J. Appl. Phys.* 105 (2009) 073301.
- [50] T. Welzel, T. Dunger, F. Richter, *Plasma Processes Polym.* 4 (2007) S931.

- [51] A. Wiatrowski, W.M. Posadowski, Z.J. Radzimski, *J. Vac. Sci. Technol. A* 26 (2008) 1277.
- [52] H. Bäcker, J.W. Bradley, P.J. Kelly, R.D. Arnell, *J. Phys. D: Appl. Phys.* 34 (2001) 2709.
- [53] P.M. Bryant, S.A. Voronin, J.W. Bradley, A. Vetushta, *J. Appl. Phys.* 102 (2007) 043302.
- [54] R. Chistyakov, B. Abraham, W.D. Sproul, J. Moore, J. Lin, Society of Vacuum Coaters 50th Annual Technical Conference Proceedings, Louisville, KY, 2007, p. 139.
- [55] M.A. Lieberman, A.J. Lichtenberg, *Principles of Plasma Discharges and Materials Processing*, John Wiley & Sons, New York, 1994.
- [56] C. Doughty, S.M. Gorbakhtin, T.Y. Tsui, G.M. Pharr, D.L. Medlin, *J. Vac. Sci. Technol. A* 15 (1997) 2623.
- [57] S.M. Rossnagel, J. Hopwood, *J. Vac. Sci. Technol. B* 12 (1994) 449.
- [58] S.M. Rossnagel, J. Hopwood, *Appl. Phys. Lett.* 63 (1993) 3285.
- [59] J.T. Gudmundsson, J. Alami, U. Helmersson, *Appl. Phys. Lett.* 78 (2001) 3427.
- [60] K. Macak, V. Kouznetsov, J.M. Schneider, U. Helmersson, I. Petrov, *J. Vac. Sci. Technol. A* 18 (2000) 1533.
- [61] F. Chen, *Introduction to Plasma Physics and Controlled Fusion*, Second Edition Plenum Press, New York, 1984.
- [62] I. Langmuir, H. Mott-Smith, *Gen. Electr. Rev.* 25 (1924) 429.
- [63] A.D. Pajdarova, J. Vlcek, P. Kudlacek, J. Lukas, *J. Phys. D: Appl. Phys.* 18 (2009) 025008.
- [64] S.-H. Seo, J.-H. In, H.-Y. Chang, *Plasma Sources Sci. Technol.* 15 (2006) 256.
- [65] J. Bohlmark, J. Alami, C. Christou, A.P. Ehiasarian, U. Helmersson, *J. Vac. Sci. Technol. A* 23 (2005) 18.
- [66] S.P. Bugaev, V.G. Podkovyrov, K.V. Oskomov, S.V. Smaykina, N.S. Sochugov, *Thin Solid Films* 389 (2001) 16.
- [67] H.R. Griem, *Plasma Spectroscopy*, McGraw-Hill, New York, 1964.
- [68] A.C.G. Mitchell, M.W. Zemansky, *Resonance Radiation and Excited Atoms*, Cambridge University Press, Cambridge, 1971.
- [69] O. Auciello, D.L. Flamm, *Plasma Diagnostics, Volume 1: Discharge Parameters and Chemistry*, Academic Press, San Diego, 1989.
- [70] S. Konstantinidis, J.P. Dauchot, M. Ganciu, A. Ricard, M. Hecq, *J. Appl. Phys.* 99 (2006) 013307.
- [71] A.P. Ehiasarian, A. Vetushta, A. Hecimovic, S. Konstantinidis, *J. Appl. Phys.* 104 (2008) 83305.
- [72] K. Sarakinos, J. Alami, C. Klever, M. Wuttig, *Rev. Adv. Mater. Sci.* 15 (2007) 44.
- [73] S. Konstantinidis, J.P. Dauchot, M. Ganciu, M. Hecq, *Appl. Phys. Lett.* 88 (2006) 021501.
- [74] L. de Poucques, J.C. Imbert, C. Boisse-Laporte, J. Bretagne, M. Ganciu, L. Teulé-Gay, M. Touzeau, *Plasma Sources Sci. Technol.* 15 (2006) 661.
- [75] J. Bohlmark, M. Lattemann, J.T. Gudmundsson, A.P. Ehiasarian, Y.A. Gonzalvo, N. Brenning, U. Helmersson, *Thin Solid Films* 515 (2006) 1522.
- [76] M. Lattemann, A.P. Ehiasarian, J. Bohlmark, P.O.Å. Persson, U. Helmersson, *Surf. Coat. Technol.* 200 (2006) 6495.
- [77] J. Andersson, A.P. Ehiasarian, A. Anders, *Appl. Phys. Lett.* 93 (2008) 071504.
- [78] S.M. Rossnagel, *J. Vac. Sci. Technol. A* 6 (1988) 19.
- [79] J. Andersson, A. Anders, *Phys. Rev. Lett.* 102 (2009) 045003.
- [80] A. Pflug, B. Szyszka, V. Sittinger, J. Niemann, Society of Vacuum Coaters 47th Annual Technical Conference Proceedings San Francisco, CA, 2003, p. 241.
- [81] R.A. Baragiola, E.V. Alonso, J. Ferron, A. Oliva - Florio, *Surf. Sci. Lett.* 90 (1979) 240.
- [82] Y.P.Y.P. Raizer, *Gas Discharge Physics*, Springer, Berlin, 1991.
- [83] L.M. Kishinevsky, *Rad. Eff.* 19 (1973) 23.
- [84] R.C. Weast, *Handbook of Chemistry and Physics*, CRC Press, Boca Raton, 1988–1989.
- [85] A. Anders, *Appl. Phys. Lett.* 92 (2008) 201501.
- [86] S.M. Rossnagel, H.R. Kaufman, *J. Vac. Sci. Technol. A* 5 (1987) 2276.
- [87] D.W. Hoffman, *J. Vac. Sci. Technol. A* 3 (1985) 561.
- [88] S. Kadlec, *Plasma Processes Polym.* 4 (2007) S149.
- [89] J.A. Bittencourt, *Fundamentals of Plasma Physics*, Third Ed Springer-Verlag, New York, 2004.
- [90] T. Hurtig, *Plasma Cloud Penetration Across Magnetic Barriers* Stockholm: Royal Institute of Technology, 2004.
- [91] J. Bohlmark, U. Helmersson, M. VanZeeland, I. Axnäs, J. Alami, N. Brenning, *Plasma Sources Sci. Technol.* 13 (2004) 654.
- [92] E. Ott, J.B. McBride, J.H. Orens, J.P. Boris, *Phys. Rev. Lett.* 28 (1972) 88.
- [93] K.B. Gylfason, J. Alami, U. Helmersson, J.T. Gudmundsson, *J. Phys. D: Appl. Phys.* 38 (2005) 3417.
- [94] F. Ze, N. Hershkowitz, C. Chan, K.E. Lonngren, *Phys. Fluids* 22 (1979) 1554.
- [95] N. Hershkowitz, T. Romesser, D. Montgomery, *Phys. Rev. Lett.* 29 (1972) 1586.
- [96] H. Ikezi, *Phys. Fluids* 16 (1973) 1668.
- [97] N. Hershkowitz, T. Romesser, *Phys. Rev. Lett.* 32 (1974) 581.
- [98] J.S. Russell, *Fourteenth Meeting of the British Association for the Advancement of Science*, 1844.
- [99] L.H. Holthuijsen, *Waves in Oceanic and Coastal Waters*, Cambridge University Press, Cambridge, 2007.
- [100] D. Lundin, U. Helmersson, S. Kirkpatrick, S. Rohde, N. Brenning, *Plasma Sources Sci. Technol.* 17 (2008) 025007.
- [101] D. Lundin, P. Larsson, E. Wallin, M. Lattemann, N. Brenning, U. Helmersson, *Plasma Sources Sci. Technol.* 17 (2008) 035021.
- [102] N. Brenning, I. Axnäs, M.A. Raadu, D. Lundin, U. Helmersson, *Plasma Sources Sci. Technol.* 17 (2008).
- [103] J. Bohlmark, M. Östbye, M. Lattemann, H. Ljungcrantz, T. Rosell, U. Helmersson, *Thin Solid Films* 515 (2006) 1928.
- [104] S. Sevana, S. Chennadi, R.K. Lakkaraju, J. Li, S. Rohde, Society of Vacuum Coaters 48th Annual Technical Conference Proceedings, Denver, CO, 2005, p. 720.
- [105] K. Bobzin, N. Bagcivan, P. Immich, S. Bolz, J. Alami, R. Cremer, J. Mater. Process. Technol. 209 (2008) 165.
- [106] W.D. Sproul, D.J. Christie, D.C. Carter, Society of Vacuum Coaters 47th Annual Technical Conference Proceedings, Dallas, TX, 2004, p. 96.
- [107] D.A. Glocker, M.M. Romach, D.J. Christie, W.D. Sproul, Society of Vacuum Coaters 47th Annual Technical Conference Proceedings, Dallas, TX, 2004, p. 183.
- [108] K. Sarakinos, J. Alami, M. Wuttig, *J. Phys. D: Appl. Phys.* 40 (2007) 2108.
- [109] J.A. Davis, W.D. Sproul, D.J. Christie, M. Geisler, Society of Vacuum Coaters 47th Annual Technical Conference Proceedings, Dallas, TX, 2004, p. 215.
- [110] J. Alami, P. Eklund, J.M. Andersson, M. Lattemann, E. Wallin, J. Bohlmark, P. Persson, U. Helmersson, *Thin Solid Films* 515 (2007) 3434.
- [111] B.M. DeKoven, P.R. Ward, R.E. Weis, D.J. Christie, R.A. Scholl, W.D. Sproul, F. Tomasel, A. Anders, Society of Vacuum Coaters 46th Annual Technical Conference Proceedings, San Francisco, CA, 2003, p. 158.
- [112] H. Weis, T. Müggenburg, P. Grosse, L. Herlitz, I. Friedrich, M. Wuttig, *Thin Solid Films* 351 (1999) 184.
- [113] P. Siemroth, T. Schülke, *Surf. Coat. Technol.* 133–134 (2000) 106.
- [114] J.H. Se, T.S. Kang, D.Y. Noh, *J. Appl. Phys.* 81 (1997) 6716.
- [115] R. Berisch, *Sputtering by Particle Bombardment I*, Springer, Berlin, 1982.
- [116] J. Emmerlich, S. Mraz, R. Snyders, K. Jiang, J.M. Schneider, *Vacuum* 82 (2008) 867.
- [117] D.J. Christie, *J. Vac. Sci. Technol. A* 23 (2005) 330.
- [118] K. Sarakinos, J. Alami, J. Dukwen, J. Wördnenweber, M. Wuttig, *J. Phys. D: Appl. Phys.* 41 (2008) 215301.
- [119] F. Ziegler, J.P. Biersack, U. Littmark, *The Stopping and Range of Ions in Solids*, Pergamon, Oxford, 1985.
- [120] J.T. Gudmundsson, *J. Phys.: Conf. Ser.* 100 (2008) 082013.
- [121] D. Horwat, A. Anders, *J. Phys. D: Appl. Phys.* 41 (2008) 135210.
- [122] W. Lotz, *Z. Phys.* A 232 (1970) 101.
- [123] Y.-K. Kim, J.-P. Desclaux, *Phys. Rev. A* 66 (2002) 012708.
- [124] W. Lotz, *Z. Phys.* 220 (1969) 466.
- [125] S. Berg, T. Nyberg, *Thin Solid Films* 476 (2005) 215.
- [126] D. Depla, R. De Gryse, *Surf. Coat. Technol.* 183 (2004) 184.
- [127] D. Severin, O. Kappertz, T. Kubart, T. Nyberg, S. Berg, A. Pflug, M. Siemers, M. Wuttig, *Appl. Phys. Lett.* 88 (2006) 161504.
- [128] W.D. Sproul, M.E. Graham, M.S. Wong, S. Lopez, D. Li, R.A. Scholl, *J. Vac. Sci. Technol. A* (1995) 1188.
- [129] E. Wallin, U. Helmersson, *Thin Solid Films* 516 (2008) 6398.
- [130] K. Sarakinos, J. Alami, C. Klever, M. Wuttig, *Surf. Coat. Technol.* 202 (2008) 5033.
- [131] D. Depla, R. De Gryse, *J. Vac. Sci. Technol. A* 20 (2002) 521.
- [132] J. Hopwood, *Ionized Physical Vapor Deposition*, Academic Press, San Diego, 2000.
- [133] W. Ensiger, *Nucl. Instrum. Method. Phys. Res. B* 127–128 (1997) 796.
- [134] C.R. Tellier, A.J. Tosser, *Size Effects in Thin Films*, Elsevier, Amsterdam, 1982.
- [135] R.C. Munoz, R. Finger, C. Arenas, G. Kremer, L. Moraga, *Phys. Rev. B* 66 (2002) 205401.
- [136] J. Alami, S. Bolz, K. Sarakinos, *Journ. All. Comp.* 483 (2009) 530.
- [137] T. Schuelke, T. Witke, H.J. Scheibe, P. Siemroth, B. Schultrich, O. Zimmer, J. Vetter, *Surf. Coat. Technol.* 120–121 (1999) 226.
- [138] J. Alami, P.O.Å. Persson, D. Music, J.T. Gudmundsson, J. Bohlmark, U. Helmersson, *J. Vac. Sci. Technol. A* 23 (2005) 278.
- [139] A.P. Ehiasarian, J.G. Wen, I. Petrov, *J. Appl. Phys.* 101 (2007) 054301.
- [140] J. Vetter, T. Michler, H. Steuernagel, *Surf. Coat. Technol.* 111 (1999) 210.
- [141] C. Schönjahn, A.P. Ehiasarian, D.B. Lewis, R. New, W.D. Münz, R.D. Twesten, I. Petrov, *J. Vac. Sci. Technol. A* 19 (2001) 1415.
- [142] G. Häkansson, L. Hultman, J.-E. Sundgren, J.E. Greene, W.-D. Münz, *Surf. Coat. Technol.* 48 (1991) 61.
- [143] A.P. Ehiasarian, W.-D. Münz, L. Hultman, U. Helmersson, I. Petrov, *Surf. Coat. Technol.* 163–164 (2003) 267.
- [144] P.E. Hovsepian, C. Reinhard, A.P. Ehiasarian, *Surf. Coat. Technol.* 201 (2006) 4105.
- [145] J.S. Koehler, *Phys. Rev. B* 2 (1970) 547.
- [146] P.M. van Attekum, P.H. Woerlee, G.C. Verkade, A.A. Hoeben, *Phys. Rev. B* 29 (1984) 645.
- [147] P. Barna, M. Adamik, *Science and Technology of Thin Films*, World Science Publishing Co. Pte. Ltd., Singapore, 1995.
- [148] J. Paulitsch, P.H. Mayrhofer, C. Mitterer, W.-D. Münz, M. Schenkel, *Society of Vacuum Coaters 50th Annual Technical Conference Proceedings*, Louisville, KY, 2007, p. 150.
- [149] J. Alami, K. Sarakinos, F. Uslu, M. Wuttig, *J. Phys. D: Appl. Phys.* 42 (2009) 015304.
- [150] A.P. Ehiasarian, P.E. Hovsepian, L. Hultman, U. Helmersson, *Thin Solid Films* 457 (2004) 270.
- [151] P. Patsalas, C. Gravalidis, S. Logothetidis, *J. Appl. Phys.* 96 (2004) 6234.
- [152] L. Hultman, J.E. Sundgren, J.E. Greene, D.B. Bergstrom, I. Petrov, *J. Appl. Phys.* 78 (1995) 5395.
- [153] H. Agura, A. Suzuki, T. Matsushita, T. Aoki, M. Okuda, *Thin Solid Films* 445 (2003) 263.
- [154] V. Sittinger, F. Ruske, W. Werner, C. Jacobs, B. Szyszka, D.J. Christie, *Thin Solid Films* 516 (2007) 5847.
- [155] I. Petrov, F. Adibi, J.E. Greene, L. Hultman, J.E. Sundgren, *Appl. Phys. Lett.* 63 (1993) 36.
- [156] L.A. Clevenger, A. Mutscheller, J.M.E. Harper, C. Cabral, K. Barmak, *J. Appl. Phys.* 72 (1992) 4918.
- [157] D.W. Face, D.E. Prober, *J. Vac. Sci. Technol. A* 5 (1987) 3408.
- [158] J. Alami, P. Eklund, J. Emmerlich, O. Wilhelmsen, U. Jansson, H. Höglberg, L. Hultman, U. Helmersson, *Thin Solid Films* 515 (2006) 1731.
- [159] M.W. Barsoum, *Prog. Solid State Chem.* 28 (2000) 201.
- [160] P. Eklund et al., *Thin Solid Films* 518 (2010) 1851.
- [161] K.K. Tominaga, D. Ito, M. Miyamoto, *Vacuum* 80 (2006) 654.
- [162] S. Mraz, J.M. Schneider, *J. Appl. Phys.* 100 (2006) 023503.
- [163] J.M. Ngaruya, O. Kappertz, S.H. Mohamed, M. Wuttig, *Appl. Phys. Lett.* 85 (2004) 748.
- [164] M.D. Wiggins, M.C. Nelson, C.R. Aita, *J. Vac. Sci. Technol. A* 14 (1996) 772.
- [165] W. Zhou, X.X. Zhong, X.C. Wu, L.Q. Yuan, Q.W. Shu, W. Li, Y.X. Xia, *J. Phys. D: Appl. Phys.* 40 (2007) 219.
- [166] J. Alami, K. Sarakinos, F. Uslu, C. Klever, J. Dukwen, M. Wuttig, *J. Phys. D: Appl. Phys.* 42 (2009) 115204.

- [167] V. Stranak, M. Quaas, H. Wulff, Z. Hubicka, S. Wrehde, M. Tichy, R. Hippeler, *J. Phys. D: Appl. Phys.* 41 (2008) 055202.
- [168] R. Bandorf, M. Vergöhl, P. Giesel, T. Wallendorf, G. Mark, Society of Vacuum Coaters 50th Annual Technical Conference Proceedings, Louisville, KY, 2007, p. 160.
- [169] D. Severin, O. Kappertz, T. Nyberg, S. Berg, M. Wuttig, *Thin Solid Films* 515 (2007) 3554.
- [170] E. Wallin, T.I. Selinder, M. Elfving, U. Helmersson, *Europhys. Lett.* 82 (2008) 36002.
- [171] Y. Yamada-Takamura, F. Koch, H. Maier, H. Bolt, *Surf. Coat. Technol.* 142 (2001) 260.
- [172] O. Zywitzki, G. Hoetzsch, F. Fietzke, K. Goedicke, *Surf. Coat. Technol.* 82 (1996) 169.
- [173] M. Arbab, *Thin Solid Films* 381 (2001) 15.



Kostas Sarakinos received his Ph.D. in physics from the RWTH University of Aachen, Germany (Institute of Physics) in 2008. In the framework of his Ph.D. he investigated the growth mechanisms in transition metal nitride films, as well as the fundamentals of high power pulsed magnetron sputtering (HPPMS). He is currently a postdoctoral researcher at the RWTH University of Aachen (Institute of Materials Chemistry), while he has been awarded a grant from the Swedish research council (VR) to join the University of Linköping, Sweden in 2010. His research interests include the fundamentals and the applications of HPPMS, the phase formation in metal oxides and oxynitrides grown by ionized physical and chemical vapor deposition techniques, and the knowledge-based materials design using ab initio calculations. He has published 20 original and review papers.



Jones Alami is the Innovation manager at Sulzer Metaplas GmbH, Bergisch Gladbach, Germany. He received his Ph.D. in materials science, in particular thin-film physics, from Linköping University, Sweden, in 2005. His thesis topic was plasma analysis and thin film deposition by high power pulsed magnetron sputtering. After a postdoctoral position in 2005–2006 at the Institute of Physics at RWTH Aachen, Germany, he joined the industry and held the positions of Research Engineer and Research manager. He has over 40 publications including a number of industrial articles.



Stephanos Konstantinidis received his Ph.D. degree in Chemistry in 2004 from the University of Mons, Belgium. His scientific interests include plasma diagnostics and thin film growth during ionized PVD processes, in particular HPPMS. He is the author of several invited lectures and articles and the coauthor of a patent related to the development of a high power pulse generator. After a Research Engineer position at Materia Nova R&D center and a postdoctoral position at the Institute of Materials Chemistry, RWTH Aachen University, Germany, he currently holds a postdoctoral position financed by the Belgian National Fund for Scientific Research (FNRS), at the University of Mons.